Tackling Recalcitrant *Pseudomonas aeruginosa* Infections In Critical Illness via Anti-virulence Monotherapy

Vijay K. Singh[1,2,3,#], Marianna Almpani[1,2,3,#], Damien Maura[1,2,3,#], Tomoe Kitao[1,2,3], Livia Ferrari[4], Stefano Fontana[5], Gabriella Bergamini[4], Elisa Calcaterra[4], Chiara Pignaffo[5], Michele Negri[6], Thays de Oliveira Pereira[7], Frances Skinner[8], Manos Gkikas[8], Danielle Andreotti[9], Antonio Felici[10], Eric Déziel[7], Francois Lépine[7], Laurence G. Rahme[1,2,3*]

[1]Department of Surgery, Harvard Medical School and Massachusetts General Hospital, Boston, USA

[2]Shriners Hospitals for Children, Boston, USA

[3]Department of Microbiology, Harvard Medical School, Boston, MA 02115, USA

[4]Translational Biology Department, Aptuit (Verona) S.rl, *an Evotec Company*, 37135 Via A. Fleming 4, Verona, Italy

[5]DMPK Department, Aptuit (Verona) S.rl, *an Evotec Company*, 37135 Via A. Fleming 4, Verona, Italy

[6]*In vitro* Chemotherapy Laboratory, Aptuit (Verona) S.r.l., *an Evotec Company*, 37135 Via A. Fleming 4, Verona, Italy

[7]Centre Armand-Frappier Santé Biotechnologie, Institut National de la Recherche Scientifique (INRS), Laval, Quebec, H7V 1B7 Canada

[8]Department of Chemistry, University of Massachusetts Lowell, Lowell, MA 01854, USA

[9]Global Synthetic Chemistry Department, Aptuit (Verona) S.r.l., *an Evotec Company*, 37135 Via A. Fleming 4, Verona, Italy

[10]Department of Microbiology Discovery, *In Vitro* Biology, Aptuit (Verona) S.r.l., *an Evotec Company*, 37135 Via A. Fleming 4, Verona, Italy

Current address:

D. Maura, Voyager Therapeutics, Cambridge, MA 02139, USA

T. Kitao, Department of Microbiology, Graduate School of Medicine, Gifu University, Gifu 501-1194, Japan

A Felici, Academic Partnership, Evotec SE, 37135 Via A. Fleming 4, Verona, Italy

[*]**Corresponding author:**

e-mail: rahme@molbio.mgh.harvard.edu (LGR)

address: Massachusetts General Hospital, 340 Their Research Building, 50 Blossom Street, Boston, MA 02114; phone: 617-724-5003

[#] These authors contributed equally

Abstract

Intestinal barrier derangement allows intestinal bacteria and their products to translocate to the systemic circulation. *Pseudomonas aeruginosa* (*PA*) superimposed infection in critically ill patients increases gut permeability and leads to gut-driven sepsis. *PA* infections are challenging due to multi-drug resistance (MDR), biofilms, and/or antibiotic tolerance. Inhibition of the quorum-sensing transcriptional regulator MvfR(PqsR) is a desirable anti-*PA* strategy as MvfR controls multiple acute and chronic virulence functions. Here we show that MvfR promotes intestinal permeability and report novel potent anti-MvfR compounds, the N-Aryl Malonamides (NAMs) resulting from extensive structure-activity-relationship studies and thorough assessment of the inhibition of MvfR-controlled virulence functions. This novel class of anti-virulence non-native ligand-based agents has a half-maximal inhibitory concentration in the nanomolar range and strong target engagement. Using a NAM lead in monotherapy protects murine intestinal barrier function, abolishes MvfR-regulated small molecules, ameliorates bacterial dissemination, and lowers inflammatory cytokines. This study demonstrates the importance of MvfR in *PA*-driven intestinal permeability. It underscores the utility of anti-MvfR agents in maintaining gut mucosal integrity, which should be part of any successful strategy to prevent/treat *PA* infections and associated gut-derived sepsis in critical illness settings. NAMs provide for the development of crucial preventive/therapeutic monotherapy options against untreatable MDR *PA* infections.

Keywords: *Pseudomonas aeruginosa*; virulence; anti-virulence; anti-infectives; intestinal permeability; critical illness; MvfR; PqsR

1. Introduction

The recalcitrant ESKAPE pathogen *Pseudomonas aeruginos*a presents a serious threat to critically ill and immunocompromised patients [1-3]. The most prevalent among the frequently colonized by *P. aeruginosa* body sites are the respiratory system, urinary tract, skin, and gastrointestinal tract [4-7]. This opportunistic pathogen's intestinal colonization, in particular, is associated with elevated mortality rates of patients in intensive care units (ICU), and its significance as a cause of mortality in critically ill patients has been demonstrated in randomized prospective studies [8,9]. Besides being an important reservoir for this pathogen, the gastrointestinal tract can be a significant source of systemic sepsis and death among critically ill patients [10,11] who inherently have defective intestinal integrity secondary to their critical clinical condition [12,13].

There is an exponentially growing body of evidence that the composition of the gut microbial flora and alterations of the commensal bacterial populations following injuries, infections, and critical illness, strongly influence our metabolic, endocrine, immune, peripheral, and central nervous systems. It is now clear that maintaining gut mucosal integrity must be part of any successful strategy to prevent/treat infections and the gut-derived sepsis syndrome seen in critical illness settings. Derangement of the intestinal barrier subsequently allows intestinal bacteria and their products to translocate to the systemic circulation. A significant number of lung infections have been reported to arise due to direct contamination of the airways by the gastrointestinal flora or by hematogenous dissemination from the intestine to the lung parenchyma [10,11,14,15]. At the same time, the crucial role of circulating microbes originating from the gut has long been recognized as a critical player in the development of multiple organ failure (MOF) in critically ill patients [16,17]. When added to the critical illness, *P. aeruginosa* infections occur, there is an exacerbation of the intestinal barrier dysfunction with even more devastating results. Indeed, *P. aeruginosa* virulence factors have been shown to further promote increased intestinal permeability [18].

Infections with *P. aeruginosa* are challenging to eradicate due to this pathogen's high antibiotic resistance [19,20]. Moreover, attempts to eradicate *P. aeruginosa* infections can fail when traditional antibiotics leave unharmed the subpopulation of bacterial cells that are refractory to antibiotics [1], which along with biofilms are ultimately responsible for chronic, and persistent/relapsing infections[21,22]. Therefore, in the post-antibiotic era, the development and implementation of new anti-microbial strategies, that would allow us to effectively tackle multi-drug resistant (MDR)

infections and the formation of antibiotic tolerant, persister (AT/P) cells are imperative. One attractive and intensely investigated anti-microbial approach is quorum sensing (QS) inhibition [23-26], a cell-cell communication signaling mechanism employed by bacteria to efficiently coordinate their behaviors, many of which are virulence-related. Bacteria, including *P. aeruginosa*, release low molecular weight molecules as chemical signals capable of concomitantly mediating the transcription of virulence genes [27] and modulating host immune responses [28-30]. QS inhibition (QSI) is neither bactericidal nor bacteriostatic. Therefore, the principle behind the QSI approach to treat severe infections is to disarm the virulent bacteria, rendering them less pathogenic for the host while simultaneously avoiding the strong selective pressure that antibiotic killing or antibiotic-mediated growth arrest entails.

The QS transcriptional regulator MvfR (multiple virulence factor regulator, also known as PqsR)[31,32] is one of the three interconnected *P. aeruginosa* QS regulators that govern many virulence functions in this pathogen [33-38] (Figure 1). MvfR plays a central role in the *P. aeruginosa* QS interplay due to its direct control of the other QS regulators, LasR and RhlR. Additionally, MvfR controls the synthesis of ~60 distinct low-molecular-weight compounds via the transcriptional regulation of the *pqsABCDE* operon [38]. The production of these small signaling molecules is responsible for the difficulty of eradicating acute, chronic, and persistent/relapsing (ACPR) infections, including acute and chronic pneumonia, relapsing and chronic wound and ear infections, as well as medical device-related infections [39]. We have shown that loss of the MvfR function completely abolishes the production of these molecules and several redox-generating molecules [36,40]. These include reduced production of pyocyanin, a redox-active molecule that causes oxidative stress in host cells and dysregulates the host immune mechanisms [30,41,42] and, importantly, 2-AA (2-aminoacetophenone) that promotes LasR mutations, AT/P cell formation, and host chromatin modifications, impacting histone acetylation. As shown in Figure 1, all these effects lead to persistent infections[30,33,34].

The ability of MvfR to control acute and chronic bacterial functions, and notably unlike LasR, the other QS regulator, no clinical isolates from patients have been reported to date to have frequent mutations in MvfR, making it a highly desirable target for drug discovery and underscoring its importance in *P. aeruginosa* pathogenesis.

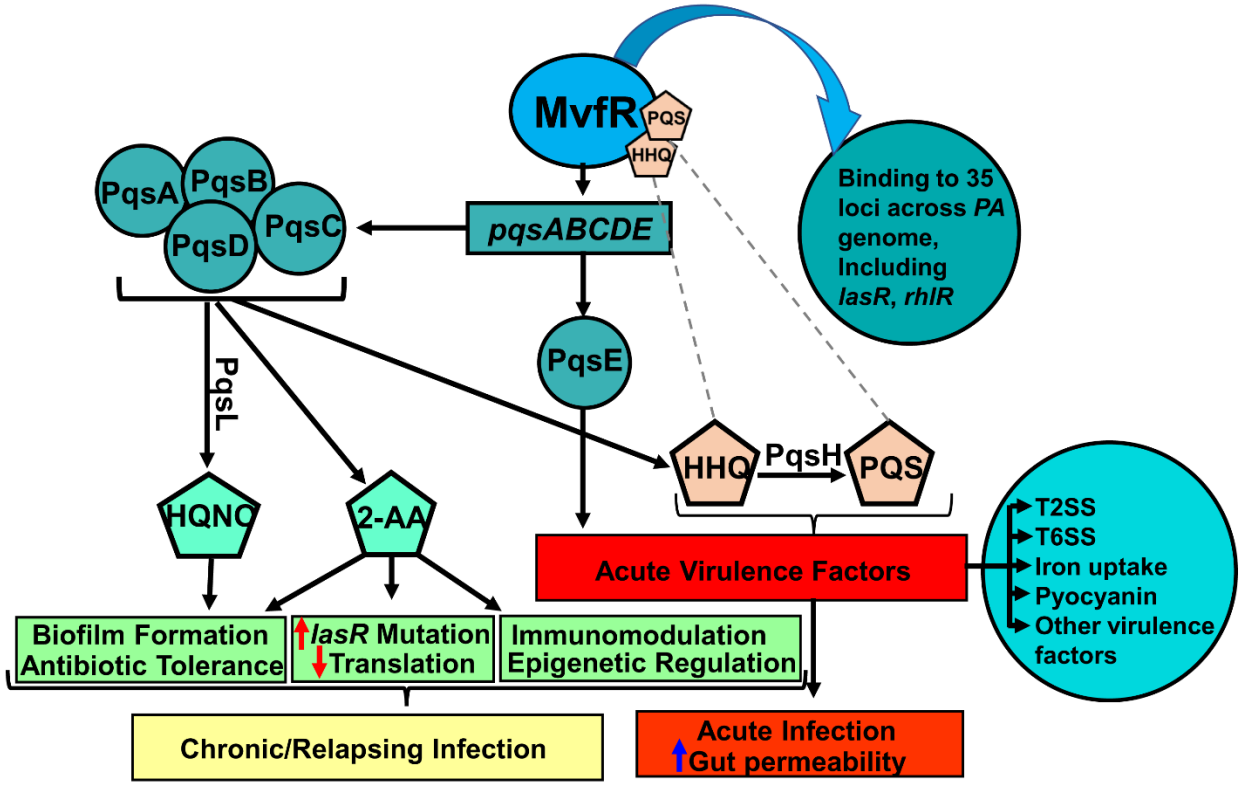

Figure 1. Current view of the *P. aeruginosa* MvfR QS system impact on acute and chronic functions. MvfR (PqsR), in the presence of its ligands/inducers PQS or HHQ, binds and activates the transcription of the *pqs* operon, whose encoded proteins catalyze the biosynthesis of ~60 compounds, including PQS, HHQ, HQNO, and 2-AA. HQNO promotes both pro-acute and pro-persistent phenotypes, while HHQ and PQS, promote acute phenotypes. 2-AA's immunomodulatory action and epigenetic regulation along with the accumulation of *lasR* mutants and the formation of AT/P cells that survive antibiotic killing contribute to persistent infections. Moreover, MvfR impacts the production of several virulence factors, including pyocyanin and binds and directly regulates the expression of 35 loci across the *P. aeruginosa* genome, including major regulators and virulence factors, such as the QS regulators LasR and RhlR, and genes involved in protein secretion, translation, and response to oxidative stress [36]. Agents that bind and inhibit MvfR function is a successful strategy to control the multiple virulence functions under MvfR control.

In this study, we focused on one of the unexplored chemical families we identified from our original whole-cell-based High-Throughput Screen (HTS) represented by the non-ligand-based

compound M17 [23] and built upon the harnessed knowledge on the MvfR function, its regulation, and inhibition [12,23,24,34,43-46]. We demonstrate the importance of MvfR in intestinal permeability and open new avenues for preclinical development of anti-MvfR agents based on the novel family of highly efficient chemical series, namely N-Aryl Malonamides (NAMs) that are compatible with *in vivo* use.

2. Results

2.1 Design and Structure-Activity Relationship (SAR) of Non-Ligand-Based anti-*MvfR* Agents

Our original whole-cell-based HTS of a chemical library of 284,256 molecules identified several chemical families of compounds with a potent anti-MvfR activity that were structurally different from the MvfR positive regulatory ligands 4-hydroxy-2-heptylquinoline (HHQ) and 3,4-dihydroxy-2-heptylquinoline (PQS) [23,35]. Previously we focused on the family of compounds containing a benzothiazole moiety and a variously substituted aromatic amide group [23] such as M64 (Figure S1A). While many of these compounds were quite active in inhibiting MvfR function, they suffered from low solubility and presented chemical liabilities that complicated their utility in an *in vivo* setting. Notably, the presence of the sulfur atom seemed problematic as it is susceptible *in vivo* to metabolism.

Here we investigated the anti-MvfR potential of another previously unexplored chemical family identified from our original HTS. Starting with compound M17 [23] and following many rounds of structure-activity relationship (SAR) studies, a total of 84 compounds were generated and tested (Table S1 A-G) to identify a novel chemical series, N-Aryl Malonamides (NAMs), as potent MvfR inhibitors non-based on the structure of the MvfR-native ligands. Given that MvfR regulates the transcription of the *pqsABCDE* operon and the production of pyocyanin, as a first step of the compounds' activity screening and prioritization, we determined their efficacy in impacting pyocyanin production and the transcription of the MvfR-regulated *pqs operon* using a *pqs*-GFP reporter construct (Table S1A-G) [47].

M17 (Table S1A and Figure S1B) shares the substituted N-Aryl amide moiety of our previously identified low soluble chemical family of anti-MvfR compounds [23]. Compared to the potent compound M64 (Figure S1 A), M17 has a 2-methyl, 4-Fluoro anilines in place of the 2-tio-benzimidazole motif and a 4-cyano instead of 4-phenoxy on the N-Aryl amide side. A series of

M17 analogs (N 2-(Arylamino)-N-arylacetamide) was generated by replacing the various substituents on both aryl-rings (Table S1A-B) without obtaining compounds significantly more active than M17. Varying the nature of the linker and the chain length between the two substituted Aryl rings (Table S1C), no particularly relevant results were observed except for D24, where the central glycinamide has been formally attached with the opposite orientation. D24 showed a similar anti-MvfR profile to D16, D28, and D33 (Table S1B), suggesting that the linker (the glycinamide) can be placed between Aryl rings in either way. That prompted us to design D36, characterized by a malonamide as a central motif, and this compound was selected for further optimization (Table S1D-G).

The most active malonamide derivatives generally share two substituents at the para position of each of the phenyl rings. These substituents usually are electron-withdrawing and/or lipophilic groups. The presence of groups such as cyano, chlorine, bromine, trifluoromethyl, nitro, or iodine on one or both aromatic rings increases the compounds' anti-MvfR activity. Substituting one phenyl ring with the lipophilic para phenoxy group led to a series of very active compounds such as D57 (Table S1D), D67, D68, D88, and D100 (Table S1E-F and Figure 1). The presence of two substituents between the two carbonyls resulted in a loss of potency for compounds D87, D94, and D97, suggesting the need to have at least one hydrogen available in the position as observed for the symmetric compounds D43 with D80. A single fluoride on that position, as in compound D96, was partially tolerated. However, when combined with a more lipophilic group (Phenoxy) by replacing one of the 4-cyano group present on the aryl gave rise to compound D88, which retained the potency and surprisingly increased the solubility (Table S2) despite having the lipophilic phenoxy substituent generally responsible of reducing solubility.

Our results show that of the 84 compounds tested, 18 compounds, D36, D41, D42, D43, D51, D56, D57, D58, D61, D62, D63, D69, D71, D95, D77, D80, D88, and D100, reduced the transcription from the *pqsA* gene expression inhibiting its transcription by $\geq$ 90% (Table S1B-F). Similarly, compounds D36, D41, D42, D43, D51, D57, D58, D60, D61, D62, D63, D69, D92, D95, D77, D80, D88, and D100 inhibited pyocyanin production also by $\geq$ 90% (Table S1A-F). None of the compounds tested affected the growth of any *P. aeruginosa* clinical isolates used in these studies (data not shown), which is characteristic of anti-virulence compounds.

To functionally validate these results, we subsequently tested the efficacy of these compounds in inhibiting the synthesis of the *pqs* operon catalyzed small excreted 4-hydroxy-2-alkylquinolines (HAQs) molecules, including its positive regulatory ligands HHQ and PQS, the biofilm-related molecule 4-hydroxy-2-heptylquinoline *N*-oxide (HQNO); and the non-HAQs, 2,4-dihydroxyquinoline (DHQ) and 2-aminoacetophenone (2-AA), in the presence of the compounds[34,35,38,48]. Table S1 shows that among the tested compounds (at 50 μM), D41, D42, D43, D51, D61, D62, D63, D69, D77, D80, D88, and D95, had the most robust inhibitory profile in agreement with their inhibitory efficacy against pyocyanin production and *pqsA* gene expression (Table S1). Specifically, HHQ, PQS, and HQNO production inhibition ranged between 89%-99%, 76%-97%, and 40%-92%, respectively. In addition, inhibition of 2-AA and DHQ production ranged between 82%-95% and 82%-96%, respectively.

Evaluation of these highly active compounds for chemical liabilities revealed that among these, 13 compounds, namely D41, D42, D43, D57, D67, D68, D69, D71, D77, D80, D88, D95, and D100, appear to bear no chemical liabilities for *in vivo* use (Table S1 A-G and Figure 1). Out of these 13 compounds, we selected for advancement the 10 most potent compounds D41, D42, D43, D57, D69, D77, D80, D88, D95, and D100, based on their inhibition profiles in all functions tested and listed in Table S1A-G.

2.2 NAMs inhibit MvfR-regulated virulence functions in the nanomolar range

To determine the compound dose-efficacy relationship, we further measured the concentration at which the 10 aforementioned compounds exert their 50% inhibitory effect on pyocyanin production assay and *pqsA* gene expression. Figure 2 shows the dose-dependent inhibition measured in the PA14 strain for all 10 compounds for both assays. The range of the IC_{50} values for the 10 compounds in the pyocyanin production was 0.15 μM – 4.07 μM. More than half of the compounds had an IC50 $\leq$1 μM (D57: 0.24 μM; D69: 0.96 μM; D88: 0.53 μM; D95: 0.90 μM; D100: 0.38 μM) with D57 having the lowest (0.24 μM) IC_{50} for pyocyanin production and D77 having the highest of all (4.07 μM) (Figure 2). For the *pqsA*-GFP expression assay, the range of the IC_{50} values was 0.43 μM–10.6 μM, with the vast majority of the compounds having an IC_{50} around or below 1μM (D41: 1.09 μM; D42: 0.92 μM; D43: 0.97 μM; D57: 0.43 μM; D69: 1.7 μM; D88: 1.31 μM; D95: 1.09 μM; D100: 0.38 μM), and the lowest IC_{50} value being observed following incubation with D57 (Figure 2).

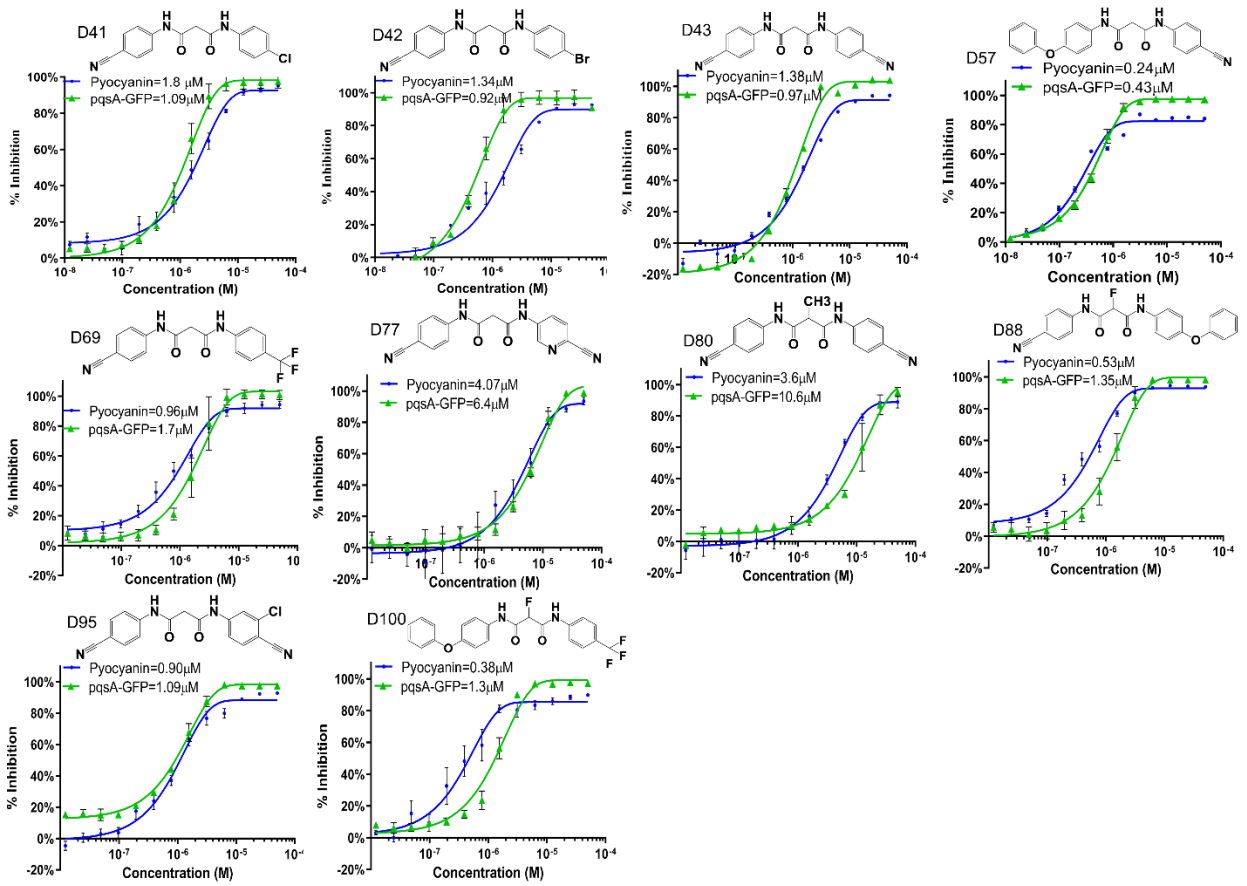

Figure 2. Dose dependent inhibition of Pyocyanin production and *PqsA-GFP* expression. IC_{50} determination was performed in the presence and absence of the 10 NAM compounds individually at 13 different concentrations ranging from 0.01 μM-50 μM. Graphs are showing IC_{50} values for pyocyanin (blue) and *PqsA-GFP* (green) for D41, D42, D43, D57, D69, D77, D80, D88, D95, D100. IC_{50}, curves were plotted as percentage of pyocyanin production and *pqsA-GFP* expression of the indicated compounds. The percentage of compound inhibition was calculated by comparing PA14 cells grown in the presence of the vehicle control. The IC_{50} values for each compound were calculated using the GraphPad Prism software. Data represent at least three independent replicates. The error bars denote ± SEM.

Sixteen MDR *P. aeruginosa* blood or wound isolates (Table S3) were used to cross-validate the efficacy of all 10 NAMs to inhibit pyocyanin production. As shown in Figure S2, all except D80 are highly efficacious against all multidrug-resistant *P. aeruginosa* clinical isolates tested. At a

concentration of 10 μM NAMs, most compounds substantially reduced pyocyanin production in these MDR *PA* clinical isolates (Figure S2).

2.3 NAMs prevent the formation of *P. aeruginosa* AT/P cells and attenuate initiation of biofilm formation

The MvfR-regulated signaling molecule 2-AA promotes the formation of the AT/P cells [33] implicated in the failure of antibiotic treatments in clinics. AT/P cells, a subpopulation of bacterial cells that survive lethal concentrations of antibiotics, can lead to persistent bacterial infections that can be the source of latent, chronic, or relapsing infections. Therefore, we further tested the efficacy of the 10 advanced NAMs against the formation of AT/P cells and compared their efficacy to the wild-type strain PA14 and isogenic mutant *mvfR*. Figure 3A shows that all 10 compounds significantly reduced the formation of AT/P cells compared to the wild-type strain PA14, agreeing with their efficacy to decrease the levels of 2-AA synthesis (Table 1A-G). Most of them provided a significant reduction similar to that observed with the *mvfR* mutant.

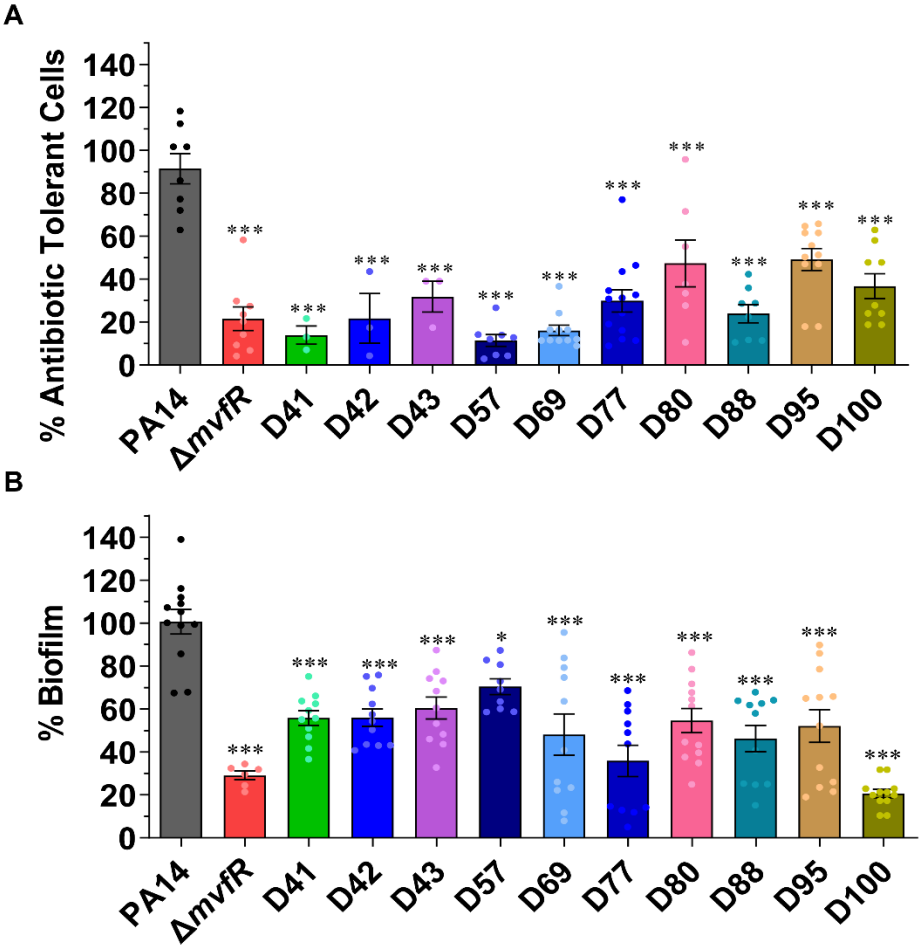

Specifically, the 5 compounds D41, D42, D57, D69, and D88 inhibit AT/P cells formation by ≥76% (76%-88%) and the rest D43, D77, D80, D95 and D100 by ≥51% (56%-70%).

Figure 3: **NAMs are potent agents against the formation of antibiotic tolerant, persisters (AT/P) cells and biofilm. (A)** AT/P cells formation in PA14 and isogenic Δ*mvfR* in the presence or absence of the indicated compounds. Cells were grown in the presence of 10 μg mL^{-1} meropenem, and/or 10 μM of the compounds for 24 h. Values were normalized to the cells grown for 4 h in the absence of antibiotics and compound. The PA14 cells grown with antibiotics and vehicle (DMSO) were considered control, and the percentage values were calculated compared to control. **(B)** Initiation of biofilm formation of PA14 and Δ*mvfR* cells with or without compound. Biofilm was grown in the 96 well microtiter plate at 37˚C for 24 h containing M63 minimal media in the presence of 10 μM of the compounds or vehicle. After 24 h, the wells were washed to remove planktonic cells, and the biofilm was stained with 0.1% crystal violet. The stained biofilm was washed and solubilized in ethanol: acetone (80:20). OD was measured at 570nm. The biofilm grown with the vehicle was considered as a control. The percentage value was calculated in comparison to the PA14 control. The error bars denote ± SEM. Statistical analysis was carried out using GraphPad Prism software. One-way ANOVA followed by Tukey post-test was applied. "∗", "∗∗" and "∗∗∗" indicate significant differences from the control at $P < 0.05$, $P < 0.01$, and $P < 0.001$, respectively. "ns" represent no significant difference.

Moreover, Figure 3B shows that initiation of biofilm formation was also significantly reduced by all the tested compounds after 24hr of growth in the presence of 10 μM of the respective compounds compared to the PA14 control strain. Specifically, 8 out of the 10 compounds, namely D41, D42, D69, D77, D80, D88, D95, and D100, showed an inhibition rate between 80%-45%, while D43, D57, D80, and D95 exerted an inhibition rate of 40%-30%. The highest inhibition was observed by compound D100 followed by compound D77 and D88.

2.4 Assessments of NAMs targeting MvfR

To further determine NAMs specificity for MvfR and exclude their potential binding to any of the Pqs operon enzymes, we tested their ability to inhibit the production of HAQs, 2-AA, and DHQ utilizing the isogenic *mvfR* mutant constitutively expressing the *pqsABCDE* operon, which leads to the production of these molecules independently of MvfR. Figure 4A shows that the

levels of these molecules are similar between all the compound-treatment groups and the vehicle-treatment control, confirming that our selected NAMs do not confer any MvfR-independent inhibition of the HAQs, 2-AA, and DHQ production by interfering with the enzymes catalyzing their synthesis. Moreover, to further assess the absence of an off-target effect with the selected NAMs for the MvfR-related phenotypes tested, we assessed the formation of AT/P cells and biofilm using the PA14 isogenic *mvfR* mutant. Figure 4B-C shows that none of the MvfR NAM inhibitors tested exhibit an off-target effect since the formation of AT/P cells and biofilm profile were similar to that of the *mvfR* mutant alone or in combination with all of the tested NAMs.

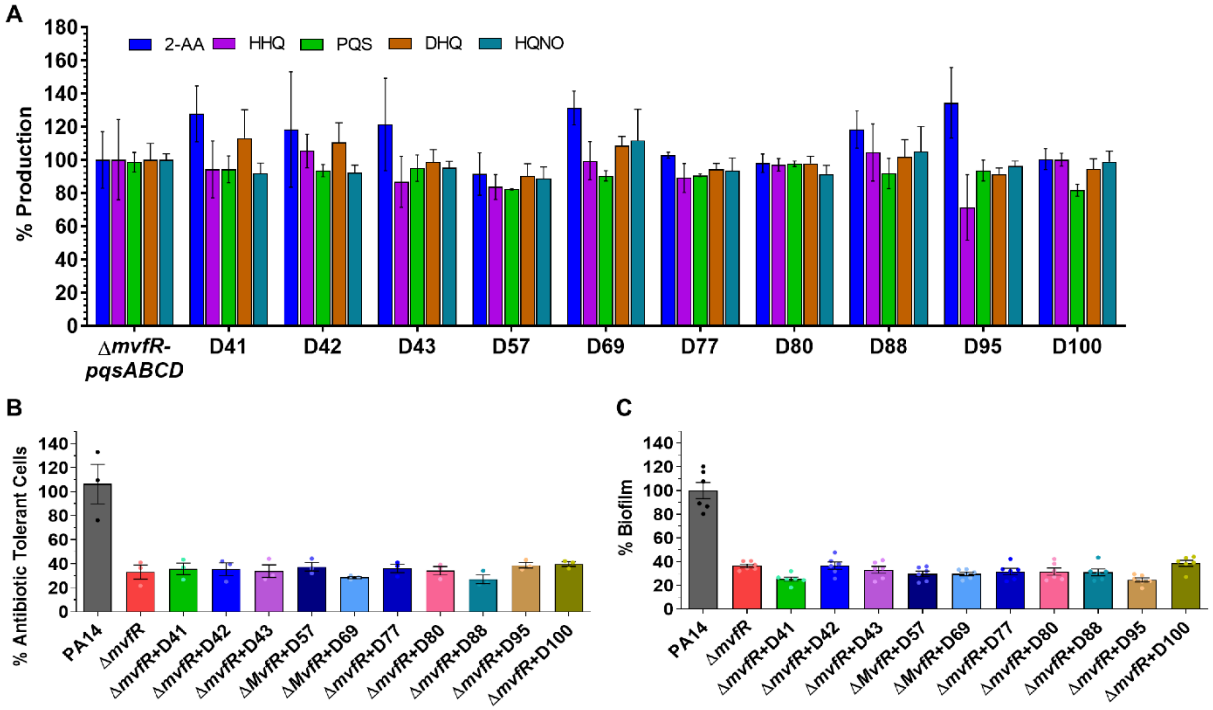

Figure 4: *In vitro* assessment of NAMs efficacy indicate no off-target effect. (A) Effect of the selected compounds on the MvfR-independent HAQs, 2-AA and DHQ production. The production of the MvfR-regulated small molecules 2-AA, HHQ, PQS, DHQ, and HQNO was measured in the cultures at OD_{600nm} = 3.0 in the presence of 50μM of the indicated compounds using a *MvfR* mutant strain that constitutively expresses the *pqsABCDE* genes. The cells were grown with or without (vehicle only) compound and the small molecules production was measured using liquid chromatography-mass spectrophotometry (LC-MS). The percentage production was calculated in comparison to cells grown with the vehicle control. **(B)** AT/P cell

formation in the PA14 isogenic mutant Δ*mvfR* in the presence of the indicated compounds. Cells were grown in the presence of 10 μg mL^{-1} meropenem, followed by adding 10 μM of the compounds for 24 h. Values were normalized to cells grown for 4h in the absence of antibiotics and compounds. The Δ*mvfR* cells grown with antibiotics and vehicle were considered control, and the percentage values were calculated compared to control. **(C)** Biofilm formation of mutant Δ*mvfR* cells with or without compound. Biofilm was grown in the 96 well microtiter plate at 37˚C for 24 h containing M63 minimal media in the presence of 10 μM of the compounds or vehicle. The biofilm grown with the vehicle was considered as a control. The percentage value was calculated in comparison to the PA14 control. The error bars denote ± SEM. Statistical analysis was carried out using GraphPad Prism software. One-way ANOVA followed by Tukey post-test was applied. "∗" and "∗∗∗" indicate significant differences from the control at $P < 0.05$ and $P < 0.001$, respectively.

Surface plasmon resonance (SPR) analysis was also performed to determine whether the advanced compounds bind MvfR and assess their binding affinity. Figure S3 shows that these compounds indeed bind MvfR with high affinity having a K_D value ranging between 0.24-1.25 μM.

Taken together, these findings show that the advanced NAMs inhibit MvfR-regulated functions by targeting MvfR.

2.5 Solubility assessment prioritizes D88 as the lead compound

Compound's low solubility can be a bottleneck in drug development. Solubility measurements using High-Performance Liquid Chromatography (HPLC) show that the 10 compounds' solubility ranged between 2 μM and 490 μM (Table S2). Although several of these 10 compounds performed consistently well in all the assays mentioned above, compound D88 displayed by far the highest solubility (490 μM) of all the tested compounds and was one of the most effective inhibitors in all assays performed. Notably, the increase in solubility observed with D88 was not observed with D100, likely due to the extra lipophilicity added by the CF_3 group replacing the Cyano. Replacing one or both aromatic groups with a pyridine, as in D77, shows low solubility (Table 1G and Table 2). Thus, we focused on D88 for further assessments prior to using it *in vivo* studies.

2.6 Additional studies supporting the prioritization of D88.

First, we assess the potency of this NAM in the inhibition of PqsABCD products by determining the IC_{50} inhibitory concentration of D88 against the production of 2-AA, HHQ, PQS, DHQ, HQNO, and AA by testing gradually increasing concentrations (0.0122 μM–50 μM) of this compound. IC_{50} measurements show D88 exerts 50% inhibition against HHQ at a concentration of 3.1 μM, PQS at a concentration of 2.1 μM, HQNO at a concentration of 1.3 μM, 2-AA at a concentration of 1.5 μM, and DHQ at a concentration of 4.14 μM (Figure 5A-B).

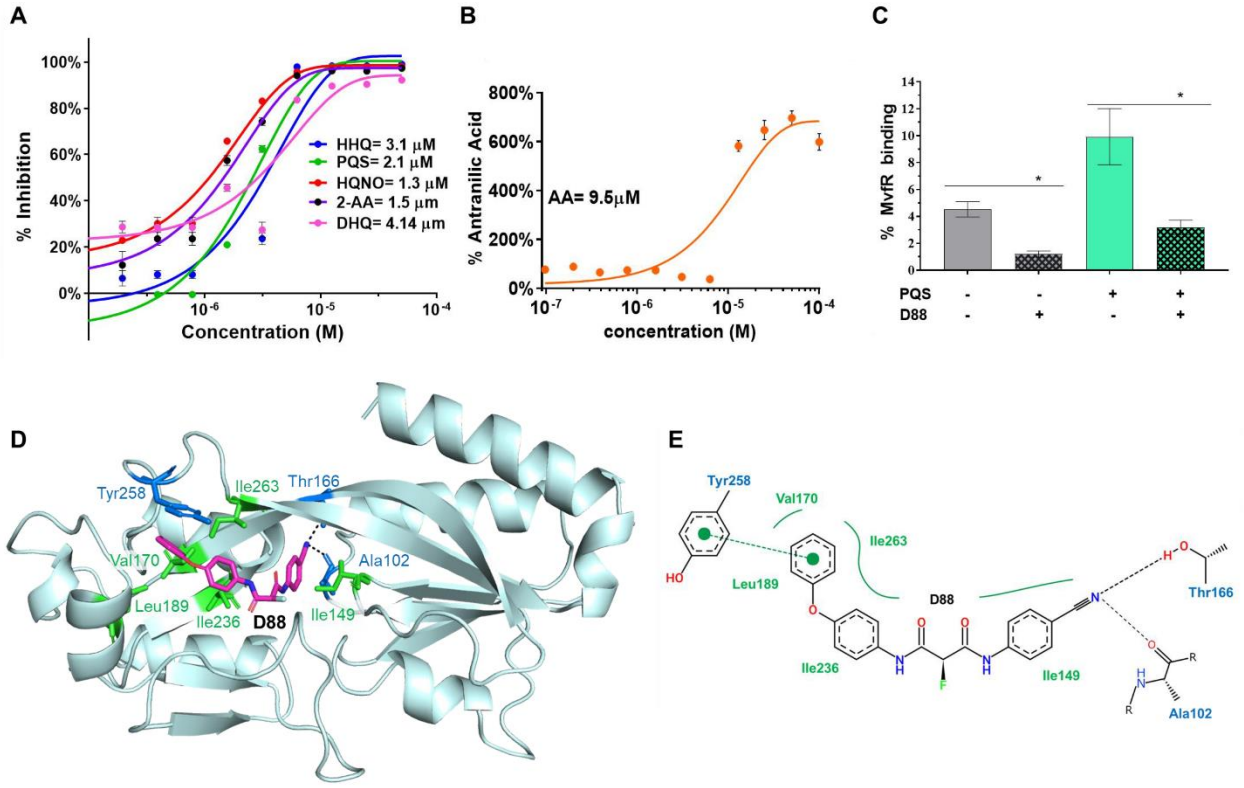

Figure 5. IC_{50} measurements, *in vitro* engagement and molecular docking studies support the prioritization of compound D88. (A) Dose-dependent inhibition of HHQ, PQS, HQNO, 2-AA, and DHQ production measured in PA14 cultures at OD_{600nm}=3.0 in the presence of 13 different concentrations of compound D88 ranging from 0.0122 μM-50 μM. The cells grown with the compound's vehicle were considered the control. **(B)** Dose-dependent production of AA (anthranilic acid) in the presence of the 13 different concentrations of D88. AA is the primary precursor of all the MvfR-regulated small molecules assessed in A. GraphPad PRISM software

plotted the IC_{50} curves against percent inhibition of the HAQs, 2-AA, DHQ, and AA (anthranilic acid) production at each concentration. **(C)** D88 inhibition of MvfR binding to the *pqsA* promoter. Overnight grown culture of PA14 expressing MvfR-VSV-G was diluted to OD 600_{nm} 0.01 and grown at 37°C with and without D88 (50 µM) and/or PQS (38 µM) until OD 600_{nm} 1.0. Thereafter MvfR-DNA complex were cross-linked and isolated via chromatin immunoprecipitation (ChIP). Coprecipitated DNA was purified and quantified using Quantitative real-time polymerase chain reaction qPCR. MvfR binding to the *pqsA* promoter was calculated using input method. Statistical analysis was carried out using GraphPad Prism software. One-way ANOVA followed by Tukey post-test was applied. "∗" indicate significant differences from the control at $P < 0.05$. **(D)** Schematic representation of D88 docking into the MvfR hydrophobic pocket. Diagram of the MvfR hydrophobic ligand-binding pocket with D88 (magenta stick). Black dashed lines indicate estimated hydrogen bonding formed between MvfR and D88. Ala102/Thr166 related to hydrogen bonding and Tyr258 related to pi-interaction are shown as blue sticks. Green sticks indicate the residues contributing to hydrophobic interactions between MvfR and D88. **(E)** Two-dimensional diagram of MvfR-D88 docking. A Green dashed line connecting two green dots indicates pi interaction. The solid green line indicates hydrophobic interactions made by hydrophobic residues (Ile149, Val170, Leu189, Ile236, and Ile263) surrounding D88. Black dashed lines indicate hydrogen bonding formed between the nitrogen of D88 and Ala102/Thr166.

The binding of MvfR protein to the *pqs* promoter is essential for activation of *pqs* operon genes transcription and the subsequent production of 60 small molecules, including the signaling molecules PQS, HHQ, and 2-AA. To determine the efficacy of D88 to disrupt MvfR binding to *pqs* operon promoter and its ability to antagonize with PQS, one of the natural ligands of MvfR [35], we used PA14 cells expressing MvfR fused to a vesicular stomatitis virus glycoprotein (VSV-G) epitope at the C-terminus grown with and without D88 at a concentration of 50 µM. The MvfR–DNA complex was isolated via chromatin immunoprecipitation (ChIP). Quantification of the co-precipitated DNA by qPCR using *mvfR* promoter-specific primers (*pqsA*) shows ~ 80% reduction of MvfR biding to the *pqs* operon promoter in the presence of 50 µM D88 as compared to the control (Figure 5C). Moreover, D88 significantly decreased the PQS–mediated increase in MvfR binding when PQS was also added exogenously (Figure 5C).

Molecular docking analysis reveals that D88, although structurally distinct from MvfR's native

ligands PQS and HHQ, targets the same hydrophobic pocket in its ligand-binding domain (LBD) (Figure 5D) as its ligands and the previously identified BB competitive inhibitor M64 [49]. The estimated free energy (ΔG) for MvfR-D88 docking is -9.6. As shown in Figure 5E, the hydrogen bonding between Ala102/Thr166 residues and the nitrogen of D88 and pi interaction between Tyr258 and the phenoxy group of D88 appears to be important in MvfR-D88 interaction.

The potential toxicity of D88 was also assessed by utilizing four different cells lines. Cell viability of the human cell lines, hepatoma Hep G2, colorectal adenocarcinoma Caco-2, lung carcinoma epithelial A549 cells, and the mouse macrophage cell line RAW 264.2 was assessed in the presence and absence of D88 at various concentrations. As shown in Figure S4, no significant changes in cell viability were detected after 24 h in any of the cell lines with any of the D88 concentrations tested compared to the vehicle control.

Finally, the drug metabolism and pharmacokinetics (DMPK) of D88 was performed to assess its half-life and bioavailability. Heathy animals received 1mg/kg intravenous (IV) and 10mg/kg subcutaneous (SC) administration of D88 and the half-life and bioavailability of the compound were assessed in the plasma at various time points. Supplementary Figure S5 shows the D88 half-life ($T_{½}$ [h]) (0.27 h and 1.25 h), T_{max} (0.08h and 0.33h), C_{max} (1,086 ng mL^{-1} and 1,096 ng mL^{-1}), and C_{last} (14.2 ng mL^{-1}, and 66.6 ng mL^{-1}) in plasma following IV and SC administration respectively.

2.7 *MvfR* promotes intestinal permeability, and its pharmacologic inhibition mitigates the host intestinal barrier damage.

Considering the importance of intestinal barrier function in health and the significance of this pathogen as a cause of mortality in critically ill patients, we interrogated the MvfR impact in intestinal permeability and the efficacy of the D88 compound in interfering with MvfR function. We used paradigmatically a well-established clinically relevant burn and infection mouse model (Figure 6A). Given that the extensive Total Burn Surface Area (TBSA) and the high inoculum used in this model exemplify the infection-related adverse outcomes in the host following acute *P. aeruginosa* infections in critically ill patients. Therefore, the results of these *in vivo* experiments could also be relevant in the setting of *P. aeruginosa* infections that are related to any type of critical illnesses, as delineated in the introduction.

Although MvfR function is required for full virulence *in vivo*, its direct role in intestinal permeability has not been demonstrated directly. We measured the FITC-dextran 3–5 kDa flux from the intestinal lumen to the systemic circulation at 22 h following burn and infection using the specific regiment shown in Figure 6A. Flux differences between the groups were determined at 22 h when the burn impact on gut permeability essentially returns to the sham levels, while the strong effect of infection on the intestinal barrier dysfunction is still observed. Figure 6B shows, that the mice that were burnt and infected with PA14 exerted a higher flux of FITC-dextran out of the intestinal lumen (mean FITC-dextran=4639 ng mL^{-1}) compared to the mice that only underwent burn injury without infection (mean FITC-dextran=1158 ng mL^{-1}; $P<0.001$). In contrast, mice infected with the PA14 isogenic *mvfR* mutant displayed a significantly decreased intestinal barrier dysfunction (mean FITC-dextran=1179 ng mL^{-1}), clearly showing the role of MvfR in intestinal permeability.

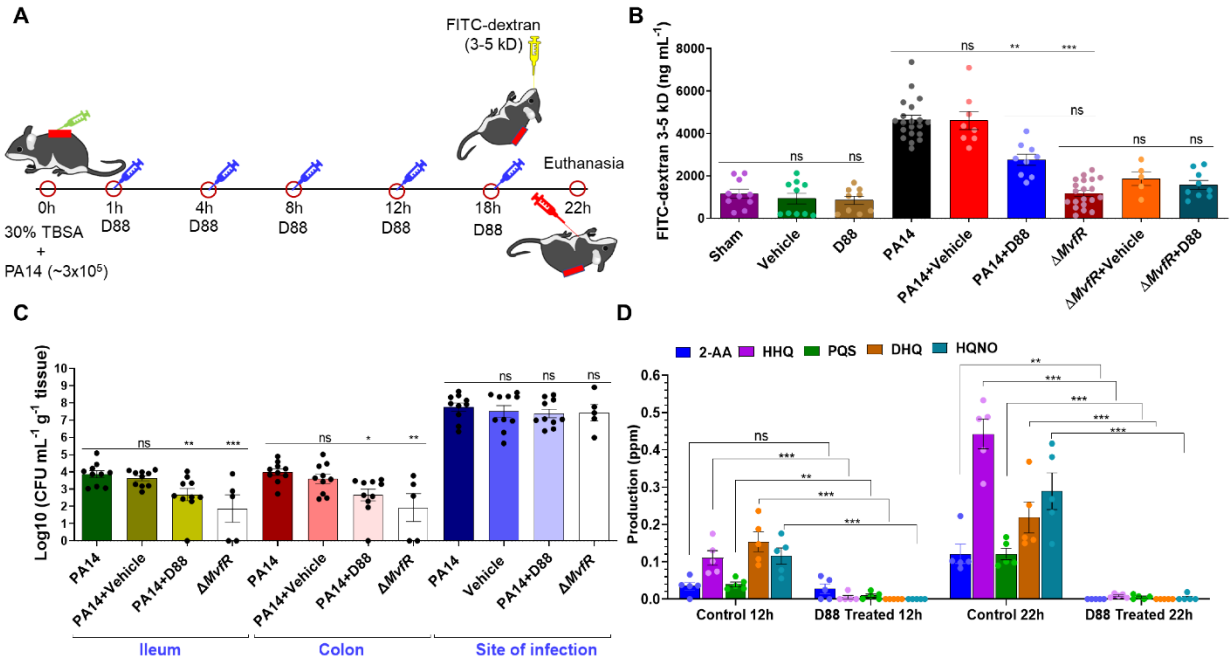

Figure 6: MvfR promotes intestinal permeability. Its pharmacologic inhibition mitigates the host intestinal barrier damage, ameliorates bacterial dissemination, and abolishes the production of the small molecules. (A) Schematic representation of the burn-site infection model and treatment plan. **(B)** Fluorescein Isothiocyanate-Dextran **(**FITC-dextran) 3-5 kDa levels in the serum 22 h post-infection. FITC-dextran 3-5 kDa was gavaged 8hr post-burn and

infection. Blood was collected 4hr following gavage (22 h post-burn and infection), and the FITC-dextran fluorescence intensity was measured using fluorescent spectrophotometry (excitation, 480 nm, and emission, 520 nm). **(C)** Effect of D88 on the bacterial dissemination to the ileum and colon and bacterial load at the site of infection. Small and large intestinal tissues, as well as muscle underlying the burn eschar and infection site from mice of each group were collected at 22 h post-burn and infection. Sample homogenates were serially diluted and plated on Pseudomonas isolation agar plates. Bacterial colony-forming units (CFUs) were counted and were normalized by the tissue weight. (**D)** D88 inhibits the production of PQS, HHQ, HQNO, DHQ, and 2-AA in the infected mice. Production was measured in samples of the underlying muscle at the site of infection. Tissue was collected at 12 h and 22 h post-infection, and these molecules were quantified using liquid chromatography-mass spectrophotometry (LC-MS). The error bars denote ± SEM. Statistical analysis was carried out using the GraphPad Prism software. One-way ANOVA followed by Tukey post-test was applied. The no treatment group data (Burn+PA14) were compared to the vehicle and the D88 treated groups. "*", "**" and "***" indicates significant differences compared to the control at $P < 0.05$, $P < 0.01$, and $P < 0.001$, respectively. "ns" represents no significant difference.

The efficacy of the highly favorable profile of the D88 compound *in vitro* is reproduced *in vivo*. Figure 6B shows that D88 significantly ameliorated the intestinal barrier dysfunction in mice following burn and infection, reducing the FITC-dextran flux in the burnt and infected mice (mean FITC-dextran=2759 ng mL^{-1}; $P<0.01$), as compared to the vehicle-treated group, which exerted a similar phenotype as the animals infected with wild type PA14 (mean FITC-dextran=4611 ng mL^{-1}). These findings demonstrate that the D88 effect in the treatment group in mitigating the PA14-mediated derangement of intestinal permeability is solely attributed to the compound itself.

Moreover, to determine whether D88 has any potential off-target effect *in vivo*, we administered D88 to mice infected with the PA14 isogenic *mvfR* mutant strain (Figure 6B). As expected, there was no difference in the intestinal permeability status between the *mvfR* mutant-infected mice treated with D88 and the *mvfR* mutant infected ones that received no treatment or those that received the vehicle control (Figure 6B). Controls represented by two additional groups, where mice only underwent burn injury without any subsequent infection and administration of D88 or

the vehicle control. None of these treatments altered the phenotype that we observed in the burn alone group of mice, with the level of FITC-dextran detected in the systemic circulation being the same as in the burnt mice that did not receive any treatment (mean FITC-dextran=1158 ng $mL^{-1}$for the no treatment group; mean FITC-dextran=850 ng mL^{-1} for the D88-treated group) (Figure 6B).

2.8 D88 ameliorates bacterial dissemination to the small and large intestine.

Intestinal hyperpermeability in bacterial infections that originate outside the intestinal lumen has previously been correlated with increased systemic bacterial load. Therefore, given the aforementioned intestinal alterations in terms of function and morphology following infection, we determined the bacterial dissemination from the site of infection to the small and large intestine of the mice in this setting. As shown in Figure 6C, PA14 disseminated in distant organs (ileum and colon) in higher numbers than the isogenic *mvfR* mutant strain, indicating the significant role of the MvfR function *in vivo* in the ability of bacteria to disseminate in different host organs. When D88 was administered, bacterial dissemination to the intestinal tissues was also significantly reduced. Administration of the vehicle control did not affect bacterial dissemination in the ileum or colon (Figure 6C).

In the same set of experiments, we assessed the bacterial load at the site of infection. Figure 6C shows that the bacterial load at the inoculation site was the same between the PA14 and the *mvfR* mutant, and it was not affected by either treatment (D88 or the vehicle control). These results corroborate our findings regarding the MvfR role in bacterial virulence *in vivo* rather than viability and indicate that inhibition of MvfR confers significant protection from systemic bacterial dissemination.

2.9 D88 shows strong target engagement *in vivo*.

To determine the ability to engage with the target *in vivo*, we assessed the levels of HHQ, PQS, HQNO, 2-AA, and DHQ in D88 treated and untreated mice at the site of infection where the bacterial burden was similarly high as in PA14 and *mvfR* (Figure 6C). Figure 6D shows the strong inhibitory efficacy of D88 at 12h with a complete abolishment of these MvfR-regulated virulence-related molecules at 22h post-infection even though the bacterial load at the site of

infection was as high as $1x10^8$ in the infected and D88 treated animals and almost identical to the CFUs of the infected + vehicle (untreated) mice (Figure 6C). This finding demonstrates the anti-virulence efficacy of D88 and indicates its strong engagement to MvfR *in vivo* over time.

2.10 D88 mitigates the morphologic alterations of the intestinal lining and attenuates intestinal inflammation.

Key regulators of the intestinal barrier function are multi-protein Tight Junction (TJ) complexes that orchestrate the paracellular intestinal permeability. Claudins and zonula occludence junctional proteins are critical modulators of intestinal barrier integrity [50]. More specifically, some junctional proteins are protective 'tightening' proteins, while others mainly contribute to intestinal permeability functions [51]. We sought to evaluate the changes of one such TJ protein, claudin-1, by exposure-matched confocal microscopy images and subsequent intensity quantification analysis. For these studies, we used ileum samples from mice that underwent burn and infection with PA14 or with the isogenic *mvfR* mutant strain in the presence or absence of D88. Figure 6A and Figure S6 shows a marked decrease in staining for claudin-1 in the PA14+vehicle infection group that received no treatment (60.41 fluorescence intensity arbitrary units (AUs)), as compared to the mice that were infected with PA14 and received D88 (142.48 AUs), as well as compared to animals that were infected with the isogenic *mvfR* mutant strain (144.58 AUs). The images show a less even distribution at the areas of cell-cell contact and an eliminated delineation of the cell periphery in the setting of PA14 infection in the absence of MvfR inhibition. On the contrary, both the *mvfR* mutant and treatment with D88 attenuate these effects, as can be appreciated in the results shown in Figures 7A. The staining for claudin-1 exhibits a more organized appearance at the periphery of the cells, with a more uniform localization at the sites of cell-cell interaction. These data indicate a considerable improvement in the morphology of the intestinal paracellular transport following MvfR silencing.

Following derangement of the intestinal barrier integrity, microbial paracellular transport out of the lumen cues an inflammatory response from the intestinal mucosa [52]. Similarly, mucosal inflammation is known to increase the TJ disruption-mediated permeability, further deranging the paracellular transport [53], leading to a vicious cycle of defective intestinal integrity. Therefore, we determined whether and how MvfR inhibition attenuates the changes in the levels of intestinal

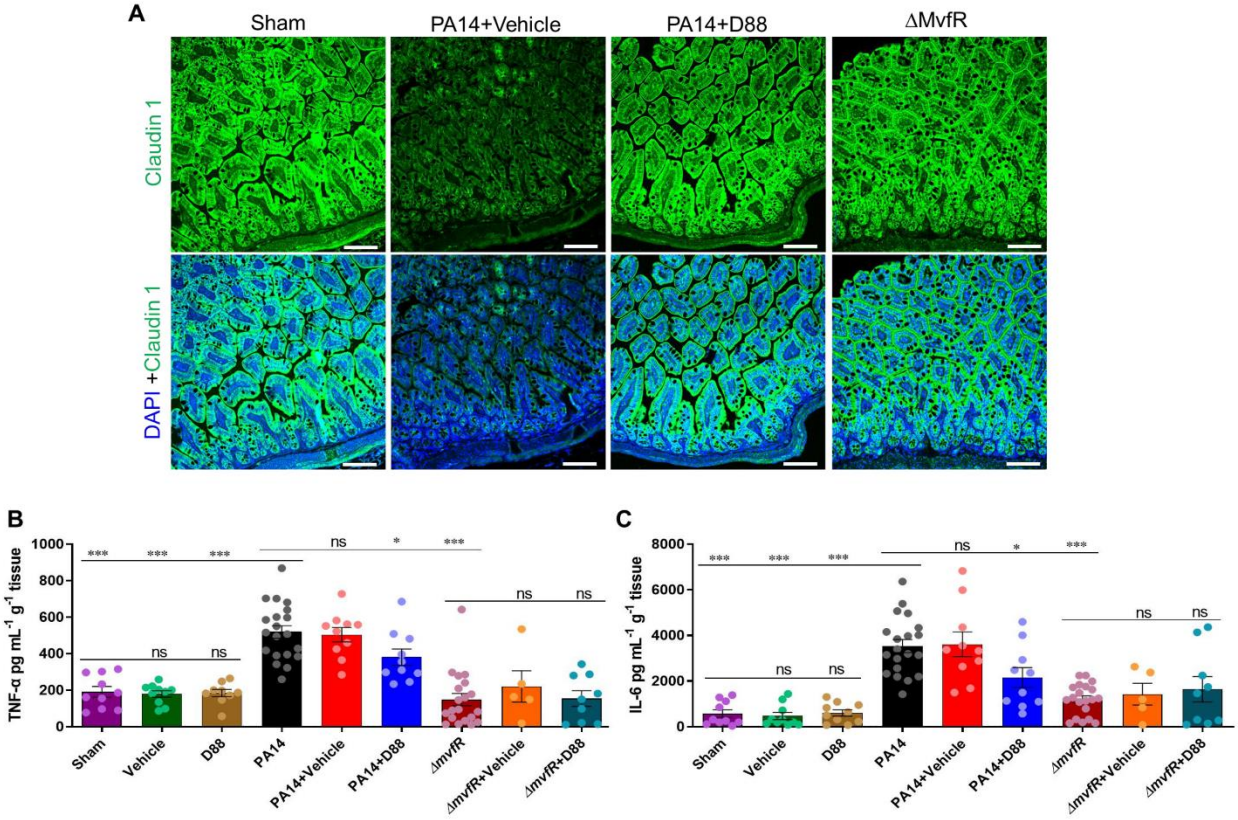

Figure 7: D88 mitigates the morphologic alterations of the intestinal lining and attenuates intestinal inflammation. (A) Representative confocal image of distal ileum with Claudin-1 immunofluorescence staining. Samples for confocal imaging were harvested 22 h post-burn and infection. Green fluorescence represents Claudin-1, and Blue fluorescence represents the DAPI stain, white line represents scale bar (100µm). **(B)** Levels of tumor necrosis factor (TNF-α) in the distal ileum 22 h post-burn and infection. The total protein was isolated from the distal ileum, and the concentration of TNF-α in the sample was quantified using ELISA. **(C)** The levels of interleukin (IL-6) in the distal ileum were also quantified using ELISA. Each dot in the bars represents one mouse. The error bars denote ± SEM. Statistical analysis was carried out using the GraphPad Prism software. One-way ANOVA followed by Tukey post-test was applied. The no treatment group data (Burn+PA14) were compared to the vehicle-treated and the D88-treated groups. "*", "**" and "***" indicates significant differences compared to the control at $P < 0.05$, $P < 0.01$, and $P < 0.001$, respectively. "ns" represents no significant deference.

inflammation in our mouse model. Figure 7B demonstrates a sharp rise of the ileal tumor necrosis factor (TNF-α) in the group that was infected with PA14 and received no treatment (mean TNF-α level of 519 pg mL^{-1} g^{-1} tissue) or received the vehicle control (mean TNF-α level of 504 pg mL^{-1} g^{-1} tissue), as compared to the burn alone group ($P<0.0001$). D88 treatment confers a significant reduction in the TNF-α levels (mean of 381 pg mL^{-1} g^{-1} tissue; $P<0.05$). The group infected with the isogenic *mvfR* mutant strain exhibited an even lower level of TNF-a, with the mean concentration being 149 pg mL^{-1} g^{-1} tissue ($P<0.0001$).

Similarly, we investigated the changes in the levels of ileal interleukin-6 (IL-6), that displayed a significant rise in the ileum of PA14-infected mice ($P<0.001$) and a marked decrease in the D88 administration group and the *mvfR* mutant infection groups ($P<0.05$ and $P<0.001$, respectively) (Figure 7C). No differences are observed between the *mvfR* infected treated and untreated animals, further demonstrating that mitigation of inflammation is not attributed to an off-target effect. The observed differences in the TNF-a and IL-6 levels further support our observation that MvfR inhibition *in vivo* significantly diminishes inflammation within the intestinal lumen. These data together highlight the importance of MvfR silencing *in vivo* as a therapeutic strategy in the setting of *PA* infections.

3. Discussion and Perspectives

P. aeruginosa colonizes the intestinal tract and aggravates the derangement of the intestinal barrier in critically ill patients who have defective intestinal integrity secondary to their primary clinical condition [12,13]. Here we demonstrate that MvfR (PqsR) represents an excellent target for limiting the ability of this pathogen to promote intestinal barrier derangement. This work is the first to report the activity of a novel NAM family of potent and effective anti-MvfR agents with a structure unrelated to the MvfR ligands/inducers PQS and HHQ and have no apparent chemical liabilities for *in vivo* use. The extensive SAR studies performed clearly show that the presence of an electron-donating phenoxy group on one of the aromatic rings leads to very active compounds. In contrast, adding a substituent at the methylene group generally results in inactive compounds except with fluorine which generates the very active compounds such as the highly soluble D88 (Table S1A-F, S2 and Figure 2). Overall, many NAM derivatives show much better solubility than the benzothiazole analogs we previously reported [23].

Several groups studying *P. aeruginosa* MvfR inhibition have so far reported compounds that show MvfR-inhibitory effects, as indicated by the repression of MvfR-regulated genes and functions *in vitro*. Among them, several plant and bacterial extracts and synthetic compounds have been used as anti-MvfR agents [54-57]. Recently Grossman et al. reported on the activity of the thiazole-containing quinazolinones inhibit MvfR function, but this was limited to the inhibition of pyocyanin *in vitro* [58]. The inhibitor, 2-((5-methyl-5H-[1,2,4]triazino[5,6-b]indol-3-yl) thio) showed efficient inhibition, and IC_{50} value was low; however, this compound was only tested for the inhibition of pyocyanin, HHQ, and PQS production *in vitro*. Another MvfR antagonist, a thioether-linked dihydropyrrol-2-one analog, was reported to inhibit biofilm formation [56]. Generating non-ligand-based MvfR-inhibiting compounds is of great importance since *P. aeruginosa* can modify ligand-based MvfR inhibitors into *MvfR* activators [59], which could ultimately increase virulence.

Especially relevant in our study is the *in vivo* monotherapy efficacy of our anti-MvfR compounds in a vertebrate *P. aeruginosa* infection model. Despite the extensive studies in *P. aeruginosa* QS inhibition over the years, the studies that report *in vivo* effects with anti-MvfR agents are few. The available *in vivo* studies that assess the impact of anti-MvfR compounds have been limited to testing these agents in non-vertebrate model hosts [60]. Though these are significant findings, the results in these model organisms might not be directly translatable to humans. Determining whether QS inhibitors are indeed effective *in vivo* and monotherapy is crucial in determining if such compounds have the potential to be incorporated in preventive or treatment approaches and strategies against *PA* infections in humans in the future. Most recently, Schütz et al. reported the inverse agonist QSI 4 for their anti-MvfR activity; the compound showed efficacy *in vitro* and has suitable pharmacokinetics (in a murine model); interestingly, however, the compound has antibacterial activity [61]. The 4-log reduction of the bacterial load at the murine infection site is the opposite of the characteristic of anti-MvfR compounds, and lack of assessment of potential off-target effect might imply that an additional QSI target might be responsible for this reduction.

Our findings also indicate that D88 is highly efficient in target engagement *in vitro* and *in vivo*. The compound appears not to have an off-target effect in the murine model tested, as shown by its efficacy in the setting of infection with the isogenic *mvfR* mutant in mice in the presence of D88, and does not target the activity of any of the *pqsABCD* operon encoded enzymes or changes

MvfR-regulated phenotypes in the setting of the *mvfR* mutant carrying the constitutively expressed *pqsABCD* operon.

The *in vivo* results show that D88 monotherapy confers significant protection against the expected *P. aeruginosa*-mediated intestinal permeability derangement. This is a significant finding given that the animal model used here represents an acute infection model in the setting of critical illness (severe burn in this instance). These results are also well correlated with the lower levels of inflammatory cytokines in the small intestine of the mice following D88 treatment compared to the no-treatment group. Additionally, despite the same bacterial load at the site of infection in all groups, we observed reduced bacterial dissemination to the intestinal tissues when MvfR was inhibited, and abolishment of the MvfR-regulated small molecules, including the MvfR inducers and signaling molecules, underscoring the impact of its pharmacologic inhibition and the importance of treating site wound infections. Reduced inflammation levels and diminished bacterial dissemination in the intestinal tissue can justify well the improved intestinal barrier function observed following compound administration.

Notably, this study carries two additional features related to the potential use of the new class of MvfR inhibitors as anti-*Pseudomonas* therapeutics. First, the herein-reported compounds are highly effective against multiple clinical *PA* isolates, showing the breadth of their efficacy beyond the PA14 strain. Second, the compound D88 reported here bears no substituents incompatible with *in vivo* use and exhibits no toxic effect following their use in macrophage and liver hepatoma cells as well as, lung and intestinal epithelial cells. The transfer of QS inhibitory compounds to clinical practice has so far been significantly limited by their cytotoxic effects or their unfavorable pharmacological properties [62]. Therefore, the favorable profile of our compounds for *in vivo* use underscores the impact and significance of this work.

Further research will be needed to address additional questions. For instance, whether the reported compounds are efficient in other infection model settings and could be used as effective adjuvants to antibiotic treatments against *PA* infections. Combining anti-MvfR agents with antibiotics may aid in reducing antibiotic doses, which could subsequently reduce the selective pressure on the pathogen to develop resistance. Nevertheless, just the loss of MvfR function completely abolishes many acute and chronic virulence-related functions [12, 15-19, 21-26] such

as those promoted by 2-AA, i.e., LasR mutations and AT/P cells formation, which also dysregulates the host immune mechanisms [30,41,46] and host chromatin modifications, leading to persistent infections [30,33,34,63].

Furthermore, even though our *in vivo* results were obtained with a vertebrate infection model, it would be useful to determine the effect of our compounds in a setting that more closely resembles human homeostasis, pathology, and pathophysiology. Recent advances in the field of organ-on-chip technology emulating native tissue architecture and the mechanochemical environment of the human tissues could be of help. Nevertheless, this work highlights the importance of maintaining gut mucosal integrity as part of any successful strategy to prevent/treat infections and the gut-derived sepsis syndrome seen in critically ill patients. Our study opens new avenues for the care of these patients.

4. Methods

4.1 Synthesis and structure modification of NAMs

Synthesis of the compound D88 was performed in three steps (Figure S6): i). to a stirred solution of compound **1** (9 g, 0.059 mol) in dichloromethane (250 mL), compound **2** (11.1 g, 0.059 mol), EDC (13.8 g, 0.071 mol), N, N-diisopropylethylamine (17 g, 0.13 mol) were added. The resulting solution was stirred at room temperature for 16 h. Then the reaction mixture was evaporated to dryness. The product was purified by column chromatography to give compound **3** (5 g, 26% yield). ii). To a stirred solution of compound **3** (5 g, 0.0157 mol) in THF and water (1:1) (200 mL), lithium hydroxide monohydrate (1.3 g, 0.031 mol) was added in one portion. The resulting mixture was stirred at room temperature for 12 h. Then the reaction mixture was acidified with 3N HCl, and the solvent was removed in vacuo; solid was filtered, washed with H_2O, and dried in vacuo to give compound **4** (4.5 g, 98% yield). iii). To a stirred solution of compound 4 (4.5 g, 0.015 mol) in DMF (150 mL), compound 5 (1.77 g, 0.015 mol), HATU (6.84 g, 0.018 mol), N, N-diisopropylethylamine (2.3 g, 0.018 mol) were added. The resulting solution was stirred at room temperature for 16 h. Then solvent was evaporated to dryness. The product was purified by column chromatography to give the title compound D88 (1.7 g, 30% yield). The route of synthesis for compound D88 is shown in Figure S2.

4.2 Bacterial strains and growth conditions

UCBPP-PA14 (PA14) is a rifampicin-resistant *P. aeruginosa* human clinical isolate (Rahme laboratory and [64]. The *mvfR* mutant is isogenic to UCBPP-PA14 (Rahme laboratory [64]. The Δ*mvfR*-pPqsABCD strain, which constitutively expresses the *pqs* operon expression, was generated by cloning the *pqsABCD* operon into pDN18 and electroporating this construct into PA14 Δ*mvfR* cells (Rahme laboratory and [23]) P*pqsA*-GFP$_{ASV}$ was previously described [47]. The *P. aeruginosa* clinical isolates LGR-4325, LGR-4326, LGR-4327, LGR-4328, LGR-4330, LGR-4331, LGR-4333, LGR-4334, LGR-4343, LGR-4344, LGR-4348, LGR-4356, LGR-4362, LGR-4363, LGR-4364, and LGR-4366 were obtained from Shriners Hospital for Children Boston, Boston MA. Unless otherwise indicated, bacteria were grown in Lysogeny Broth (LB) broth, LB agar plates, or LB agar plates containing 100 μg mL^{-1} rifampicin.

To start each assay unless otherwise specified, bacterial cells were streaked from a -80°C stock on an LB agar plate at 37°C. A single bacterial colony was then inoculated in LB medium and grown at 37°C overnight and used as a starter culture diluted 1:1000 for an over-day culture grown at 37°C to the desired optical density (OD) for the assay used.

4.3 Pyocyanin production assay

The over-day culture was grown to OD$_{600nm}$ 1.5., diluted again at 1:10,000 in 5 mL LB and incubated with 10 μM of the test compound or the vehicle control for 18 hours at 37°C and 200 rpm in an incubator shaker. After 18h, 1 mL of culture was centrifuged for 2min at 20.000 x *g*. The supernatant was transferred to a new tube, 200 μL of this were loaded in a flat-bottom 96-well plate, and the pyocyanin levels were quantified by measuring at OD$_{690nm}$. The same procedure was also followed for the pyocyanin production assessment for all the *P. aeruginosa* clinical isolates assessed in this study. The percent of pyocyanin was calculated in comparison to PA14 culture that was grown in the absence of compounds.

For the determination of the IC$_{50}$ of pyocyanin production, we followed the same process as above. Dose-dependent inhibition of pyocyanin production was performed by incubating the bacterial cultures with 13 different concentrations of each tested compound (50 μM, 25 μM, 12.5 μM, 6.25 μM, 3.125 μM, 1.562 μM, 0.781 μM, 0.390 μM, 0.195 μM, 0.0976 μM, 0.0488 μM, 0.0244 Mm and 0.0122 μM). Using GraphPad Prism Software, the IC$_{50}$ curve was plotted against percent

656 inhibition of pyocyanin production at each concentration using PA14 in absence of compounds as
657 a control.

658 **4.4 Effect of compounds on the expression of *pqsA-GFP***

659 The expression levels of *pqsA*, which is representative of the *pqsABCDE* operon transcription,
660 were monitored in the presence of the MvfR inhibitors using PA14 cells containing the P*pqsA*-
661 GFP_{ASV} , a reporter construct of the pqsA promoter fused to a short half-life GFP gene in , such
662 that quantitative quenching of fluorescence corresponds to *pqsA* promoter repression [23,34,47]. The
663 PA14 P*pqsA*-GFP_{ASV} cells were grown in 96 well plates in the presence of 10µM of the inhibitory
664 compounds and incubated at 37°C in the Infinite F200 plate reader (Sunrise Tecan, Switzerland).
665 GFP fluorescence levels were measured at λ_{ex}= 485_{nm} / λ_{em}= 535_{nm} after 10 seconds of shaking
666 every 15min up to 12h. The IC_{50} of P*pqsA-GFP* expression levels was performed as above using
667 the same 13 different concentrations (0.0122 µM–50 µM) for each of the 13 compounds tested.
668 The IC_{50} curve was plotted against percent inhibition of the *pqsA-GFP* expression at each
669 concentration, using GraphPad Prism software.

670 **4.5 Antibiotic Tolerant/ Persister (AT/P) cells formation assay**

671 The AT/P cell formation assay was performed according to the method previously described in
672 Starkey *et al.*, 2014 (persister cell assay). The over-day culture was incubated at 37°C with shaking
673 at 200rpm until the culture OD_{600nm} was 3.0. The culture was then diluted at 1:100 and grown in
674 the same conditions for 4h. After 4h, 200 uL were collected and serial dilutions were plated on LB
675 agar plates for CFU quantification (as normalizers). The remainder of the culture was treated with
676 meropenem to a final concentration of 100×MIC (Minimum Inhibitory Concentration; 10 mg L^{-1}),
677 and compounds at a final concentration of 10 µM. After 24 hours culture aliquots were 10-fold
678 serially diluted in LB broth and plated on LB agar for CFU quantification. The AT/P fraction was
679 determined as the normalizers (pre-antibiotic) ratio divided by AT/P fraction (24 h post-antibiotic)
680 [23].

681 **4.6 Assessment of biofilm formation in 96-well plates**

682 The overnight grown starter culture was diluted 1:1000 in 5 mL LB media in a glass tube and
683 was incubated at 37°C and 200rpm in an incubator shaker until the culture reached an OD_{600nm}

3.0. The culture was then diluted at 1:100 in M63 minimal media supplemented with 0.2% glucose, 0.5% Casamino Acids, and 1 mM $MgSO_4$. Initiation of the Biofilm formation was performed in the 96 well plates, 200ul of diluted culture was added in the wells with (10 µM) or without compounds. The cultures were allowed to grow at 37^{o}C in static conditions for 24 hours. Thereafter, planktonic culture was removed from the wells, and wells were washed three times with distilled water (DW). Biofilm was stained with 0.1% crystal violet and incubated for 15 min at room temperature (RT). Access dye was removed from the wells and washed off three times with DW and 200 uL ethanol: acetone (80:20) was added to the wells. The plate was incubated for 30min at RT and the OD was measured by spectrophotometry at 570 nm (Tecan, Switzerland). Percent biofilm formation was calculated in comparison to PA14 culture that was grown in the absence of compounds.

4.7 Production of 4-hydroxy-2-alkylquinolines (HAQs), 2-aminoacetophenone (2-AA), 2,4-dihydroxyquinoline (DHQ).

The HAQs HHQ, PQS and HQNO, as well as non-HAQs: 2-AA, and DHQ produced by PA14 cells were quantified in the presence of NAMs. The overnight grown starter culture was diluted 1:100 in 5 mL LB media in a glass tube and was allowed to grow in the presence (50 uM) or absence of compound at 37°C and 200 rpm in an incubator shaker until OD_{600} was 3. Bacterial cultures were subsequently mixed 1:1 (400 µL: 400 µL) with 100% methanol containing 20 ppm (20 µg mLl^{-1}) of tetradeutero-PQS (PQS-D4) and 10 ppm of tetradeutero-HHQ (HHQ-D4) in a 1.5 mL Eppendorf tube. The mixture was vortexed for 5 seconds and spun down for 5 minutes at 12,000 x *g*. A 700 µL aliquot of the supernatant was removed and stored in glass vials at -20^{o}C until further liquid chromatography-mass spectrophotometry (LC/MS) analysis as previously described in Lepine et al., 2003 [65]. LC/MC analysis was performed using a Micromass Quattro II triple quadrupole mass spectrometer (Micromass Canada, Pointe-Claire, Canada) in positive electrospray ionization mode, interfaced to an HP1100 HPLC equipped with a 4.5 × 150-mm reverse-phase C8 column.

4.8 Binding affinity of compounds to the MvfR protein

The selected compounds were tested for their ability to bind to MvfR. Target validation was carried out by using surface plasmon resonance (SPR). The MvfRC87 protein purified as in Xiao et. al.,

2006 [35] was covalently immobilized on a CM7 Series S sensor chip using an amine coupling reagent kit (GE Healthcare) at the range level of 3,000 to 5,000 response units (RU). RU was analyzed by Biacore T200 evaluation software 2.0 (GE Healthcare). The relative response units (RUs) at 5 seconds before the end of association were extracted from the double-reference-corrected sensor grams at different concentrations. These responses were plotted against their respective concentrations for MvfR inhibitor alone and in the presence of native MvfR ligand PQS and compared to the calculated responses for the mixture expected for different binding sites [49]

4.9 Measurement of compounds' solubility

Solubility of the 10mM compounds dissolved in DMSO was tested in the isotonic phosphate buffer (iPBS) at pH 7.4 using High-Performance Liquid Chromatography (HPLC). For the preparation of iPBS phosphate buffered saline tab (Sigma-Aldrich 08057-12Tab-F) is dissolved in 500 mL of deionized water and the final composition of the solution contains 10 mM PBS, 2.7 mM KCl, 140 mM NaCl and 0.05% Tween. A total 10 µL of the compound from a 10 mM stock solution in DMSO was added to the vial, and 190 µL of buffer was added in each vial and mixed with shaking at room temperature for 4 h. Thereafter the samples were filtered and 160 µL of the sample mixed with 40 µL of DMSO for the final injection. Ibuprofen (high solubility) and Progesterone (low Solubility) were used as standard compounds. Ammonium Acetate aqueous solution (50 mM, pH 7.4) and the acetonitrile were used as mobile phases A and B, respectively. The measurement of concentration was achieved by comparing of UV absorbance of the sample solution and the known standard solution following an HPLC separation using a generic fast gradient method. The solubility of each compound is expressed by the ratio of compound amount in the sample test solution to the amount of compound in the standard solution

4.10 Cytotoxicity assessment

For the determination of cytotoxicity, cell viability was determined using the MTT (3-[4, 5-dimethyl-2-thiazolyl]-2, 5-diphenyl-2H-tetrazolium bromide) assay in the presence and absence of compound (D88). Four different cell types, namely RAW 264.7 (macrophage), Caco-2 (colon epithelial cells), Hep G2 (liver cells), and A549 (lung epithelial cells), were grown at 37°C, 5% CO_2, in Dulbecco's Modified Eagle Medium (DMEM) or Eagle's Minimal Essential Medium (EMEM) containing 10% Fetal Bovine Serum (FBS), 2 mM glutamine, and antibiotic-antimycotic

until 80-90% confluency was reached in 96-well plates. The cells were then treated with either vehicle or different concentrations of D88 (10, 20, 30, 40, and 50 µM) for 24 h at 37°C and 5% CO_2. After 24 h, the cells were washed three times with PBS and were incubated in 200 µL PBS containing 200µg mL^{-1} MTT (Sigma-Aldrich) in a 96-well culture plate for 2 h at 37°C and 5% CO_2. Following incubation, the supernatant was discarded, and the cells were lysed in 95% isopropanol and 5% formic acid. Absorbance was measured at OD_{570nm} by spectrophotometry (Tecan, Switzerland).

4.11 *In Silico* docking of MvfR-D88.

Molecular docking was carried out using Mypresto software (https://www.mypresto5.jp/). The structure of MvfR ligand-binding domain in complex with M64 (PDB ID: 6B8A) was used to examine whether D88 fits into the same pocket where the native ligands and M64 bind [49]. The docking results were visualized on the Pymol software and the interaction forms of MvfR-D88 were analyzed using PoseView [66].

4.12 Determination of IC_{50} of the compound D88 for the HAQs, 2-AA, and DHQ production

As above, HHQ, PQS, HQNO, 2-AA, and DHQ production in bacterial cultures was assessed in presence of 13 different concentrations of D88 (50 µM, 25 µM, 12.5 µM, 6.25 µM, 3.125 µM, 1.562 µM, 0.781 µM, 0.390 µM, 0.195 µM, 0.0976 µM, 0.0488 µM, 0.0244 µM and 0.0122 µM). GraphPad PRISM software was used to plot the IC_{50} curve against the percent inhibition of these small molecules' production at each concentration.

4.13 Assessment of MvfR binding to *pqsA* promoter using Chromatin immunoprecipitation (ChIP)

The D88 inhibition of MvfR binding to *pqsA* promoter was evaluated using PA14 expressing MvfR fused to a vesicular stomatitis virus glycoprotein (VSV-G) epitope at the C-terminus [23]. Overnight grown culture of PA14 expressing MvfR-VSV-G stain were diluted to an OD_{600nm} 0.01 and grown at 37°C with and without D88 50 µM and/or PQS (38 µM) and allow the cells to grow until OD_{600nm} reached 1.0. Thereafter MvfR-DNA complex were cross-linked and isolated via

chromatin immunoprecipitation (ChIP). Coprecipitated DNA was purified (using DNA purification kit, Qiagen, USA) and quantified using quantitative real-time polymerase chain reaction qPCR. *pqsA* specific oligonucleotides were used for quantification, and the percentage of MvfR binding to the promoter was calculated using input method. Non-MvfR regulated *rpoD* promoter was used as a negative control [23,36].

4.14 Drug Metabolism and Pharmacokinetics (DMPK) of the D88 in mice

Experiments were conducted by Aptuit (Verona) S.rl, *an Evotec Company* in Italy. Six weeks old male CD-1 mice were obtained from Charles River Laboratories, Italy. Mice were maintained on a 12 h light cycle with *ad libitum* access to rodent feed and water.

Healthy animals received IV 1.0 mg kg^{-1} or SC administration of the 10.2 mg kg^{-1} in homogeneous suspension in 0.5 % HPMC in water at the volume of 1.7 mL kg^{-1}. Following administration, blood samples were collected under deep isoflurane anesthesia from the cava vein of each mouse into tubes with K3EDTA, thoroughly but gently mixed and placed on wet ice. Within 0.5 h of collection, blood was centrifuged (2500 g for 10 min at 4°C) and, within 0.5 h, aliquots of plasma were transferred into appropriately labeled sample tubes. A first 20 µL aliquot were mixed with 80 µL of Hepes 0.1 N. A second 5 µL aliquot of plasma was added to a well plate for urea quantification without dilution. Plasma samples were processed using a method based on protein precipitation with acetonitrile followed by HPLC/MS-MS analysis with an optimized analytical method.

4.15 Ethics statement

Animal protocols were reviewed and approved by the Institutional Animal Care and Use Committee (IACUC) at the MGH (protocol no. 2006N000093) and are in strict accordance with the guidelines of the Committee on Animals of the MGH, Harvard Medical School (Boston, USA), and the regulations of the Subcommittee on Research Animal Care of the MGH and the National Institutes of Health. Animals were euthanized according to the guidelines of the Animal Veterinary Medical Association. All efforts were made to minimize suffering. All experiments involving animals for PK studies were carried out by Aptuit (Verona) S.rl, *an Evotec Company*, Italy in accordance with the European directive 2010/63/UE governing animal welfare and protection,

798 which is acknowledged by the Italian Legislative Decree no 26/2014 and according to the company
799 policy on the care and use of laboratories animals. All the studies were revised by the Animal
800 Welfare Body and approved by Italian Ministry of Health (authorization n. -PR)

801 **4.16 Infection and D88 treatment studies in mice.**

802 Eight-week-old male C57BL/6 mice were purchased from the Jackson Laboratories. Mice were
803 maintained in a specific pathogen-free (SPF) environment at the Massachusetts General Hospital
804 (MGH; Boston, USA), in a 12h light 12h dark photoperiod at an ambient temperature of 22±1°C,
805 with food and water access *ad libitum*.

806 Prior to burn injury, all mice were anesthetized using one 500 µl intraperitoneal (IP) injection of
807 ketamine (125 mg kg^{-1}) and xylazine (12.5 mg kg^{-1}) in normal saline (N/S), and the dorsal fur was
808 subsequently removed with an electric clipper. A 30% total body surface area (TBSA) dorsal burn
809 was induced by immersion in 90°C water for 8 sec, using a polystyrene foam template, as in the
810 well-established burn model described by Walker and Mason (1968), with some modifications [67].
811 Spinal protection from the thermal injury was achieved by a dorsal subcutaneous injection of 500
812 µL N/S, before the induction of the burn injury. Fluid resuscitation was achieved by an
813 intraperitoneal injection of 500 µL N/S.

814 Immediately after burn injury, 100 µL of 10 mM $MgSO_4$ containing approximately $3x10^5$ colony
815 forming units (CFUs) of *PA* clinical isolate PA14 culture or isogenic *mvfR* mutant culture were
816 intradermally injected at the burn eschar of mice in the burn plus infection (BI) group. Mice in the
817 burn-alone groups received an equivalent injection of 100 µL of 10 mM $MgSO_4$. After the
818 experiment, all animals were returned to their cages to allow recovery from anesthesia. All cages
819 were kept on heating pads during this period to prevent hypothermia. Food and hydrogel on the
820 cage floor were provided *ad libitum*[68].

821 For the group supplemented with our MvfR-inhibiting compound (D88), mice received five
822 subcutaneous injections (at the nape of the animals) at 1, 4, 8, 12, and 18 h post-BI, at a dose of
823 24 mg kg^{-1} body weight. D88 was prepared in a 40% Captisol vehicle. Control groups received
824 equivalent doses of 40% Captisol vehicle.

4.17 *In vivo* intestinal permeability assay

For the assessment of the intestinal barrier function, 4 h before euthanasia, mice were gavaged with 0.2 ml of Fluorescein Isothiocyanate-Dextran (FITC-Dextran; 3–5 kDa; cat. no. FD4; Sigma-Aldrich; Merck KGaA, Darmstadt, Germany) in PBS, so that a dose of 440 mg kg^{-1} body weight was achieved. 22 h post-BI, mice were euthanized. The aseptic cardiac puncture was performed to obtain blood samples. The collected blood was stored in BD microtainer SST amber blood collection tubes on ice and then centrifuged at 15,000 g for 90 seconds. The serum was removed and was used to assess the FITC levels with fluorescent spectrophotometry (excitation, 480 nm, and emission, 520 nm)[68].

4.18 Tissue harvesting

Immediately after euthanasia, ileum and colon samples were aseptically harvested through a midline laparotomy. The intestine samples were flushed three times with sterile PBS. For future analysis, the samples were either snap-frozen in liquid nitrogen and stored at −80°C or stored in 4% paraformaldehyde.

The entire small and large intestine and the muscle underlying the burn eschar were aseptically harvested in different experiments. The samples were immediately homogenized in 1mL sterile PBS using a tissue homogenizer (Polytron, PT 10-35), and the homogenate was serially diluted and plated on Pseudomonas-isolation agar plates. Following plating, all plates were incubated at 37°C, CFUs were quantified after 24-36 h, and the counts were normalized by tissue weight.

4.19. Production of HHQ, PQS, HQNO, 2-AA, and DHQ *in vivo*

For the measurement of the production of HHQ, PQS, HQNO, 2-AA, and DHQ *in vivo*, underlying muscle from the site of infection was collected at 12 h, and 22 h post-infection, and the small molecules were extracted by homogenizing them immediately in 1mL sterile PBS as above. A 500 µL of the sample was mixed with an equal volume of methanol containing 10 ppm of HHQ-D4 and 20 ppm of PQS-D4, spun down for 5min, and 700 µL of supernatant were put in glass vials. Liquid chromatography-mass spectrophotometry (LC/MC) analysis was performed as described above and in [65].

4.20 Tight Junction (TJ) Immunofluorescence Assay

Samples of distal ileum fixed with 4% paraformaldehyde were cut in sections and mounted on microscope slides. After deparaffinization and antigen retrieval (Antigen Retrieval reagent; R&D Systems, Minneapolis, MN, USA), tissue sections were immersed in PBS/0.1 tween for 10 min and were blocked by Normal Goat Serum. They were then incubated with primary antibody rabbit polyclonal anti-claudin-1 (Catalog# 51-9000; RRID: AB_2533916; final concentration, 1:100; Invitrogen, Rockford, IL, USA) overnight in a humid chamber at 4°C. The sections were washed three times with PBS, and secondary antibody goat anti-rabbit (Catalog# ab150077; RRID: AB_2630356; final concentration: 1:500; Abcam, Cambridge, MA, USA) and DAPI (Catalog# ab228549; Abcam, Cambridge, MA, USA) were added and incubated 1-h at room temperature. The sections were then washed three times with PBS, dried, and mounted, and images were collected using a confocal microscope (Nikon ECLIPSE Ti2; Nikon Instruments Inc., Tokyo, Japan).

4.21 Intestinal inflammation assessment

Distal ileal TNF-α and IL-6 were quantified using the mouse TNF-α enzyme-linked immunosorbent assay [ELISA] Ready-SET-Go kit (eBioscience; San Diego, CA, USA) and the Mouse IL-6 DuoSet ELISA (R&D Systems) respectively, as per the manufacturer's instructions.

4.23 Statistical analysis

Triplicate samples were used for all assays, and all experiments were repeated at least twice, using 5 mice in each group. The statistical significance among groups was determined using one-way analysis of variance (ANOVA), with multiple post-hoc comparisons using Dunnett's test (Graphpad Software, La Jolla, CA, USA). A $P<0.05$ was considered statistically significant.

Acknowledgments:

This study was supported by the Massachusetts General Hospital Research Scholar Award and grant R01AI134857 to LGR. VKS was in part supported by IUSSTF-SERB Indo-U.S Postdoctoral Fellowship. MA was supported by the Shriners Hospitals Research Fellowship #84313. We thank Dr. Kelsey Wheeler for the critical reading of the manuscript and Dr. Yuji O. Kamatari for the technical advice on molecular docking analysis and Enamine for compounds' synthesis. The funders had no role in study design, data collection, interpretation, or the decision to submit the work for publication.

Conflicts of interest:

LGR has a financial interest in Spero Therapeutics, a company developing therapies to treat bacterial infections. LGR's financial interests are reviewed and managed by Massachusetts General Hospital and Partners Health Care in accordance with their conflict-of-interest policies. The rest of the authors declare no competing interests.

887 **References:**

888 1 Aliaga, L., Mediavilla, J. D. & Cobo, F. A clinical index predicting mortality with
889 Pseudomonas aeruginosa bacteraemia. *J Med Microbiol* **51**, 615-701, doi:10.1099/0022-
890 1317-51-7-615 (2002).

891 2 Maeda, T. *et al.* Quorum quenching quandary: resistance to antivirulence compounds.
892 *ISME J* **6**, 493-501, doi:10.1038/ismej.2011.122 (2012).

893 3 CDC. (ed CDC) (2019).

894 4 Harris, A. D. *et al.* Pseudomonas aeruginosa Colonization in the Intensive Care Unit:
895 Prevalence, Risk Factors, and Clinical Outcomes. *Infect Control Hosp Epidemiol* **37**, 544-
896 548, doi:10.1017/ice.2015.346 (2016).

897 5 Cohen, R. *et al.* A prospective survey of Pseudomonas aeruginosa colonization and
898 infection in the intensive care unit. *Antimicrob Resist Infect Control* **6**, 7,
899 doi:10.1186/s13756-016-0167-7 (2017).

900 6 Hoang, S. *et al.* Risk factors for colonization and infection by Pseudomonas aeruginosa in
901 patients hospitalized in intensive care units in France. *PLoS One* **13**, e0193300,
902 doi:10.1371/journal.pone.0193300 (2018).

903 7 Morin, C. D., Deziel, E., Gauthier, J., Levesque, R. C. & Lau, G. W. An Organ System-
904 Based Synopsis of Pseudomonas aeruginosa Virulence. *Virulence* **12**, 1469-1507,
905 doi:10.1080/21505594.2021.1926408 (2021).

906 8 Blair, P. *et al.* Selective decontamination of the digestive tract: a stratified, randomized,
907 prospective study in a mixed intensive care unit. *Surgery* **110**, 303-309; discussion 309-
908 310 (1991).

909 9 de Jonge, E. *et al.* Effects of selective decontamination of digestive tract on mortality and
910 acquisition of resistant bacteria in intensive care: a randomised controlled trial. *Lancet* **362**,
911 1011-1016, doi:10.1016/S0140-6736(03)14409-1 (2003).

912 10 Marshall, J. C., Christou, N. V. & Meakins, J. L. The gastrointestinal tract. The "undrained
913 abscess" of multiple organ failure. *Ann Surg* **218**, 111-119, doi:10.1097/00000658-
914 199308000-00001 (1993).

915 11 Osmon, S., Ward, S., Fraser, V. J. & Kollef, M. H. Hospital mortality for patients with
916 bacteremia due to Staphylococcus aureus or Pseudomonas aeruginosa. *Chest* **125**, 607-616,
917 doi:10.1378/chest.125.2.607 (2004).

918 12 Adiliaghdam, F. *et al.* Targeting bacterial quorum sensing shows promise in improving
919 intestinal barrier function following burnsite infection. *Mol Med Rep* **19**, 4057-4066,
920 doi:10.3892/mmr.2019.10071 (2019).

921 13 Adiliaghdam, F. *et al.* Targeting the gut to prevent sepsis from a cutaneous burn. *JCI*
922 *Insight* **5**, doi:10.1172/jci.insight.137128 (2020).

923 14 Alverdy, J. C., Aoys, E. & Moss, G. S. Effect of commercially available chemically defined
924 liquid diets on the intestinal microflora and bacterial translocation from the gut. *JPEN J*
925 *Parenter Enteral Nutr* **14**, 1-6, doi:10.1177/014860719001400101 (1990).

15 Alverdy, J. C., Aoys, E. & Moss, G. S. Total parenteral nutrition promotes bacterial translocation from the gut. *Surgery* **104**, 185-190 (1988).

16 Doig, C. J. *et al.* Increased intestinal permeability is associated with the development of multiple organ dysfunction syndrome in critically ill ICU patients. *Am J Respir Crit Care Med* **158**, 444-451, doi:10.1164/ajrccm.158.2.9710092 (1998).

17 Frink, M., Andruszkow, H., Zeckey, C., Krettek, C. & Hildebrand, F. Experimental trauma models: an update. *J Biomed Biotechnol* **2011**, 797383, doi:10.1155/2011/797383 (2011).

18 Zaborina, O. *et al.* Identification of multi-drug resistant Pseudomonas aeruginosa clinical isolates that are highly disruptive to the intestinal epithelial barrier. *Ann Clin Microbiol Antimicrob* **5**, 14, doi:10.1186/1476-0711-5-14 (2006).

19 Hancock, R. E. & Speert, D. P. Antibiotic resistance in Pseudomonas aeruginosa: mechanisms and impact on treatment. *Drug Resist Updat* **3**, 247-255, doi:10.1054/drup.2000.0152 (2000).

20 Yayan, J., Ghebremedhin, B. & Rasche, K. Antibiotic Resistance of Pseudomonas aeruginosa in Pneumonia at a Single University Hospital Center in Germany over a 10-Year Period. *PLoS One* **10**, e0139836, doi:10.1371/journal.pone.0139836 (2015).

21 Lewis, K. Persister cells. *Annu Rev Microbiol* **64**, 357-372, doi:10.1146/annurev.micro.112408.134306 (2010).

22 Boucher, H. W. *et al.* Bad bugs, no drugs: no ESKAPE! An update from the Infectious Diseases Society of America. *Clin Infect Dis* **48**, 1-12, doi:10.1086/595011 (2009).

23 Starkey, M. *et al.* Identification of anti-virulence compounds that disrupt quorum-sensing regulated acute and persistent pathogenicity. *PLoS pathogens* **10**, e1004321, doi:10.1371/journal.ppat.1004321 (2014).

24 Lesic, B. *et al.* Inhibitors of pathogen intercellular signals as selective anti-infective compounds. *PLoS pathogens* **3**, 1229-1239, doi:10.1371/journal.ppat.0030126 (2007).

25 Defoirdt, T. Quorum-Sensing Systems as Targets for Antivirulence Therapy. *Trends Microbiol* **26**, 313-328, doi:10.1016/j.tim.2017.10.005 (2018).

26 Zucca, M. & Savoia, D. The post-antibiotic era: promising developments in the therapy of infectious diseases. *Int J Biomed Sci* **6**, 77-86 (2010).

27 Miller, M. B. & Bassler, B. L. Quorum sensing in bacteria. *Annu Rev Microbiol* **55**, 165-199, doi:10.1146/annurev.micro.55.1.165 (2001).

28 Romero, M., Muro-Pastor, A. M. & Otero, A. Quorum sensing N-acylhomoserine lactone signals affect nitrogen fixation in the cyanobacterium Anabaena sp. PCC7120. *FEMS Microbiol Lett* **315**, 101-108, doi:10.1111/j.1574-6968.2010.02175.x (2011).

29 Williams, P., Winzer, K., Chan, W. C. & Camara, M. Look who's talking: communication and quorum sensing in the bacterial world. *Philos Trans R Soc Lond B Biol Sci* **362**, 1119-1134, doi:10.1098/rstb.2007.2039 (2007).

30 Bandyopadhaya, A., Tsurumi, A., Maura, D., Jeffrey, K. L. & Rahme, L. G. A quorum-sensing signal promotes host tolerance training through HDAC1-mediated epigenetic reprogramming. *Nat Microbiol* **1**, 16174, doi:10.1038/nmicrobiol.2016.174 (2016).

31 Rahme, L. G. *et al.* Use of model plant hosts to identify Pseudomonas aeruginosa virulence factors. *Proceedings of the National Academy of Sciences of the United States of America* **94**, 13245-13250, doi:10.1073/pnas.94.24.13245 (1997).

32 Cao, H. *et al.* A quorum sensing-associated virulence gene of Pseudomonas aeruginosa encodes a LysR-like transcription regulator with a unique self-regulatory mechanism. *Proceedings of the National Academy of Sciences of the United States of America* **98**, 14613-14618, doi:10.1073/pnas.251465298 (2001).

33 Que, Y. A. *et al.* A quorum sensing small volatile molecule promotes antibiotic tolerance in bacteria. *PLoS One* **8**, e80140, doi:10.1371/journal.pone.0080140 (2013).

34 Kesarwani, M. *et al.* A quorum sensing regulated small volatile molecule reduces acute virulence and promotes chronic infection phenotypes. *PLoS pathogens* **7**, e1002192, doi:10.1371/journal.ppat.1002192 (2011).

35 Xiao, G. *et al.* MvfR, a key Pseudomonas aeruginosa pathogenicity LTTR-class regulatory protein, has dual ligands. *Mol Microbiol* **62**, 1689-1699, doi:10.1111/j.1365-2958.2006.05462.x (2006).

36 Maura, D., Hazan, R., Kitao, T., Ballok, A. E. & Rahme, L. G. Evidence for Direct Control of Virulence and Defense Gene Circuits by the Pseudomonas aeruginosa Quorum Sensing Regulator, MvfR. *Sci Rep* **6**, 34083, doi:10.1038/srep34083 (2016).

37 Deziel, E. *et al.* The contribution of MvfR to Pseudomonas aeruginosa pathogenesis and quorum sensing circuitry regulation: multiple quorum sensing-regulated genes are modulated without affecting lasRI, rhlRI or the production of N-acyl-L-homoserine lactones. *Mol Microbiol* **55**, 998-1014, doi:10.1111/j.1365-2958.2004.04448.x (2005).

38 Deziel, E. *et al.* Analysis of Pseudomonas aeruginosa 4-hydroxy-2-alkylquinolines (HAQs) reveals a role for 4-hydroxy-2-heptylquinoline in cell-to-cell communication. *Proceedings of the National Academy of Sciences of the United States of America* **101**, 1339-1344, doi:10.1073/pnas.0307694100 (2004).

39 Tolker-Nielsen, T. Pseudomonas aeruginosa biofilm infections: from molecular biofilm biology to new treatment possibilities. *APMIS Suppl*, 1-51, doi:10.1111/apm.12335 (2014).

40 Hazan, R. *et al.* Auto Poisoning of the Respiratory Chain by a Quorum-Sensing-Regulated Molecule Favors Biofilm Formation and Antibiotic Tolerance. *Curr Biol* **26**, 195-206, doi:10.1016/j.cub.2015.11.056 (2016).

41 Choi, W. *et al.* Exendin-4 restores airway mucus homeostasis through the GLP1R-PKA-PPARgamma-FOXA2-phosphatase signaling. *Mucosal Immunol* **13**, 637-651, doi:10.1038/s41385-020-0262-1 (2020).

42 Bandyopadhaya, A., Singh, V. K., Chakraborty, A., Tzika, A. A. & Rahme, L. G., doi:10.1101/2021.10.03.462785 (2021).

43 Maura, D. *et al.* Polypharmacology Approaches against the Pseudomonas aeruginosa MvfR Regulon and Their Application in Blocking Virulence and Antibiotic Tolerance. *ACS Chem Biol* **12**, 1435-1443, doi:10.1021/acschembio.6b01139 (2017).

44 Allegretta, G. *et al.* In-depth Profiling of MvfR-Regulated Small Molecules in Pseudomonas aeruginosa after Quorum Sensing Inhibitor Treatment. *Front Microbiol* **8**, 924, doi:10.3389/fmicb.2017.00924 (2017).

45 Maura, D. & Rahme, L. G. Pharmacological Inhibition of the Pseudomonas aeruginosa MvfR Quorum-Sensing System Interferes with Biofilm Formation and Potentiates Antibiotic-Mediated Biofilm Disruption. *Antimicrob Agents Chemother* **61**, doi:10.1128/AAC.01362-17 (2017).

46 Bandyopadhaya, A. *et al.* The quorum sensing volatile molecule 2-amino acetophenon modulates host immune responses in a manner that promotes life with unwanted guests. *PLoS pathogens* **8**, e1003024, doi:10.1371/journal.ppat.1003024 (2012).

47 Yang, L. *et al.* Effects of iron on DNA release and biofilm development by Pseudomonas aeruginosa. *Microbiology (Reading)* **153**, 1318-1328, doi:10.1099/mic.0.2006/004911-0 (2007).

48 Lepine, F. *et al.* PqsA is required for the biosynthesis of 2,4-dihydroxyquinoline (DHQ), a newly identified metabolite produced by Pseudomonas aeruginosa and Burkholderia thailandensis. *Biol Chem* **388**, 839-845, doi:10.1515/BC.2007.100 (2007).

49 Kitao, T. *et al.* Molecular Insights into Function and Competitive Inhibition of Pseudomonas aeruginosa Multiple Virulence Factor Regulator. *MBio* **9**, doi:10.1128/mBio.02158-17 (2018).

50 Gunzel, D. & Yu, A. S. Claudins and the modulation of tight junction permeability. *Physiol Rev* **93**, 525-569, doi:10.1152/physrev.00019.2012 (2013).

51 Markov, A. G., Veshnyakova, A., Fromm, M., Amasheh, M. & Amasheh, S. Segmental expression of claudin proteins correlates with tight junction barrier properties in rat intestine. *J Comp Physiol B* **180**, 591-598, doi:10.1007/s00360-009-0440-7 (2010).

52 Michielan, A. & D'Inca, R. Intestinal Permeability in Inflammatory Bowel Disease: Pathogenesis, Clinical Evaluation, and Therapy of Leaky Gut. *Mediators Inflamm* **2015**, 628157, doi:10.1155/2015/628157 (2015).

53 Bruewer, M. *et al.* Proinflammatory cytokines disrupt epithelial barrier function by apoptosis-independent mechanisms. *J Immunol* **171**, 6164-6172, doi:10.4049/jimmunol.171.11.6164 (2003).

54 Singh, V. K., Mishra, A. & Jha, B. 3-Benzyl-Hexahydro-Pyrrolo[1,2-a]Pyrazine-1,4-Dione Extracted From Exiguobacterium indicum Showed Anti-biofilm Activity Against Pseudomonas aeruginosa by Attenuating Quorum Sensing. *Front Microbiol* **10**, 1269, doi:10.3389/fmicb.2019.01269 (2019).

55 Mok, N., Chan, S. Y., Liu, S. Y. & Chua, S. L. Vanillin inhibits PqsR-mediated virulence in Pseudomonas aeruginosa. *Food Funct* **11**, 6496-6508, doi:10.1039/d0fo00046a (2020).

56 Sabir, S. *et al.* Thioether-linked dihydropyrrol-2-one analogues as PqsR antagonists against antibiotic resistant Pseudomonas aeruginosa. *Bioorg Med Chem* **31**, 115967, doi:10.1016/j.bmc.2020.115967 (2021).

57 Zhou, J. W. *et al.* Metabolomic analysis of quorum sensing inhibitor hordenine on Pseudomonas aeruginosa. *Appl Microbiol Biotechnol* **103**, 6271-6285, doi:10.1007/s00253-019-09878-w (2019).

58 Grossman, S. *et al.* Novel quinazolinone inhibitors of the Pseudomonas aeruginosa quorum sensing transcriptional regulator PqsR. *Eur J Med Chem* **208**, 112778, doi:10.1016/j.ejmech.2020.112778 (2020).

59 Lu, C., Maurer, C. K., Kirsch, B., Steinbach, A. & Hartmann, R. W. Overcoming the unexpected functional inversion of a PqsR antagonist in Pseudomonas aeruginosa: an in vivo potent antivirulence agent targeting pqs quorum sensing. *Angew Chem Int Ed Engl* **53**, 1109-1112, doi:10.1002/anie.201307547 (2014).

60 Wang, S. *et al.* Inhibition of Virulence Factors and Biofilm Formation by Wogonin Attenuates Pathogenicity of Pseudomonas aeruginosa PAO1 via Targeting pqs Quorum-Sensing System. *Int J Mol Sci* **22**, doi:10.3390/ijms222312699 (2021).

61 Schutz, C. *et al.* A New PqsR Inverse Agonist Potentiates Tobramycin Efficacy to Eradicate Pseudomonas aeruginosa Biofilms. *Adv Sci (Weinh)* **8**, e2004369, doi:10.1002/advs.202004369 (2021).

62 Song, Y. *et al.* Inhibition of staphyloxanthin virulence factor biosynthesis in Staphylococcus aureus: in vitro, in vivo, and crystallographic results. *J Med Chem* **52**, 3869-3880, doi:10.1021/jm9001764 (2009).

63 Hoffman, L. R. *et al.* Pseudomonas aeruginosa lasR mutants are associated with cystic fibrosis lung disease progression. *J Cyst Fibros* **8**, 66-70, doi:10.1016/j.jcf.2008.09.006 (2009).

64 Rahme, L. G. *et al.* Common virulence factors for bacterial pathogenicity in plants and animals. *Science* **268**, 1899-1902, doi:10.1126/science.7604262 (1995).

65 Lepine, F., Deziel, E., Milot, S. & Rahme, L. G. A stable isotope dilution assay for the quantification of the Pseudomonas quinolone signal in Pseudomonas aeruginosa cultures. *Biochim Biophys Acta* **1622**, 36-41, doi:10.1016/s0304-4165(03)00103-x (2003).

66 Stierand, K., Maass, P. C. & Rarey, M. Molecular complexes at a glance: automated generation of two-dimensional complex diagrams. *Bioinformatics* **22**, 1710-1716, doi:10.1093/bioinformatics/btl150 (2006).

67 Walker, H. L. & Mason, A. D., Jr. A standard animal burn. *J Trauma* **8**, 1049-1051, doi:10.1097/00005373-196811000-00006 (1968).

68 Singh, V. K., Almpani, M. & Rahme, L. G. The Role of Common Solvents against Pseudomonas aeruginosa-Induced Pathogenicity in a Murine Burn Site Infection Model. *Microbiol Spectr* **9**, e0023321, doi:10.1128/Spectrum.00233-21 (2021).